by micellar nanocarriers followed by their light-induced activation at the target site might ensure the safety and effectiveness of *in vivo* gene and siRNA therapy. At present, this strategy could be applied only to the tissues, to which a visible light is accessible; however, recent advances in the laser technology such as a two-photon excitation laser (Oh et al. 1997) will solve the problems of limited tissue penetration of the light in the near future. We are now investigating *in vivo* PCI-mediated gene delivery using polymeric micelles via systemic administration and the results will be reported in a forthcoming paper.

Acknowledgements

The authors wish to express their gratefulness to the Health and Labor Sciences Research Grants in Research on Advanced Medical Technology in Nanomedicine Area from the Ministry of Health, Labor and Welfare (MHLW), Japan. Also, they wish to express their thanks for the Grant-in-Aid for Scientific Research, the Special Coordination Funds for Promoting Science and Technology and the Project on the Materials Development for Innovative Nano-Drug Delivery Systems from the Ministry of Education, Culture, Sports, Science and Technology (MEXT), Japan.

References

Bae Y, Nishiyama N, Fukushima S, Koyama H, Matsumura Y, Kataoka K. 2005. Preparation and biological characterization of polymeric micelle drug carriers with intracellular pH-triggered drug release property: Tumor permeability, controlled subcellular drug distribution, and enhanced *in vivo* antitumor efficacy. Bioconjug Chem 16:122–130.

Berg K, Selbo PK, Prasmikaite L, Tjelle TE, Sandvig K, Moan J, Gaudernack G, Fodstad O, Kjølsrud S, Anholt H, Rodal GH, Rodal SK, Høgset A. 1999. Photochemical internalization: A novel technology for delivery of macromolecules into cytosol. Cancer Res 59:1180–1183.

Elbashir SM, Harborth J, Lendeckel W, Yalcin A, Weber K, Tuschl T. 2001. Duplexes of 21-nucleotide RNAs mediate RNA interference in cultured mammalian cells. Nature 411:494–498.

Fukushima S, Miyata K, Nishiyama N, Kanayama N, Yamasaki Y, Kataoka K. 2005. PEGylated polyplex micelles from triblock catiomers with spatially ordered layering of condensed pDNA and buffering units for enhanced intracellular gene delivery. J Am Chem Soc 127:2810–2811.

Harada A, Kataoka K. 1995. Formation of polyion complex micelles in an aqueous milieu from a pair of oppositely charged block copolymers with poly(ethylene glycol) segments. Macromolecules 28:5294–5299.

Harada-Shiba M, Yamauchi K, Harada A, Shimokado K, Kataoka K. 2002. Polyion complex micelles as a vector for gene therapy—pharmacokinetics and *in vivo* gene transfer-. Gene Ther 9:407–414.

Høgset A, Prasmickaite L, Tjelle TE, Berg K. 2000. Photochemical transfection: A new technology for light-induced, site-directed gene delivery. Hum Gene Ther 11:869–880.

Høgset A, Prasmickaite L, Hellum M, Engesæter BØ, Olsen VM, Tjelle TE, Wheeler CJ, Berg K. 2002. Photochemical transfection: A technology for efficient light-directed gene delivery. Somat Cell Mol Genet 27:97–113.

Høgset A, Prasmickaite L, Selbo PK, Hellum M, Engesæter BØ, Bondted A, Berg K. 2004. Photochemical internalization in drug and gene delivery. Adv Drug Deliv Rev 56:95–115.

Ideta R, Tasaka F, Jang W-D, Nishiyama N, Zhang G-D, Harada A, Yanagi Y, Tamaki Y, Aida T, Kataoka K. 2005. Nanotechnology-based photodynamic therapy for neovascular disease using a supramolecular nanocarrier loaded with a dendritic photosensitizer. Nano Lett 5:2426–2431.

Itaka K, Yamauchi K, Harada A, Nakamura K, Kawaguchi H, Kataoka K. 2003. Polyion complex micelles from plasmid DNA and poly(ethylene glycol)–poly(L-lysine) block copolymer as serum-tolerable polyplex system: Physicochemical properties of micelles relevant to gene transfection efficiency. Biomaterials 24:4495–4506.

Itaka K, Miyata K, Harada A, Kawaguchi H, Nakamura K, Kataoka K. 2004. Clinically available endosomolytic agent for gene delivery. In: Svenson S, editor. Carrier-based drug delivery. 879. Washington: ACS Symposium Series. p 154–159.

Jang W-D, Nishiyama N, Zhang G-D, Harada A, Jiang D-L, Kawauci S, Morimoto Y, Kikuchi M, Koyama H, Aida T, Kataoka K. 2005. Suparmolecular nanocarrier of anionic dendrimer porphyrins with PEGylated cationic block copolymer to enhance intracellular photodynamic efficacy. Angew Chem Int Ed 44:419–423.

Kataoka K, Kwon GS, Yokoyama M, Okano T, Sakurai Y. 1993. Block copolymer micelles as vehicles for drug delivery. J Control Release 24:119–132.

Kataoka K, Harada A, Nagasaki Y. 2001. Block copolymer micelles for drug delivery: Design, characterization and biological significance. Adv Drug Deliv Rev 47:113–131.

Katayose S, Kataoka K. 1997. Water-soluble polyion complex associates of DNA and poly(ethylene glycol)–p(L-lysine) block copolymer. Bioconjug Chem 8:702–707.

Kwon GS, Suwa S, Yokoyama M, Okano T, Sakurai Y, Kataoka K. 1994. Enhanced tumor accumulation and prolonged circulation times of micelle-forming poly(ethylene oxide-aspartate) block copolymer–Adriamycin conjugate. J Control Release 29:17–23.

Macdonald IJ, Dougherty TJ. 2001. Basic principle of photodynamic therapy. J Porphyrins Phthalocynanines 5: 105–129.

Merdan T, Kopecek J, Kissel T. 2002. Prospects for cationic polymers in gene and oligonucleotide therapy against cancer. Adv Drug Deliv Rev 54:715–758.

Miyata K, Kakizawa Y, Nishiyama N, Harada A, Yamasaki Y, Koyama H, Kataoka K. 2004. Block catiomer polyplexes with regulated densities of charge and disulfide cross-linking directed to enhance gene expression. J Am Chem Soc 126: 2355–2361.

Moan J, Berg K, Anholt A, Madslien K. 1994. Sulfonated aluminum phthalocyanines as sensitizers for photochemotherapy. Effects of small doses on localization, dye fluorescence and photosensitivity in V79 cells. Int J Cancer 58:865–870.

Ng ACH, Li X, Ng DKP. 1999. Synthesis and photophysical properties of nonaggregated phthalocyanines bearing dendritic substitutes. Macromolecules 32:5292–5298.

Nishiyama N, Stapert HR, Nagano T, Takasu D, Jiang D-L, Aida T, Kataoka K. 2003a. Light-harvesting ionic dendrimer porphyrins as new photosensitizers for photodynamic therapy. Bioconjug Chem 14:58–66.

Nishiyama N, Okazaki S, Cabral H, Miyamoto M, Kato Y, Sugiyama Y, Nishio K, Matsumura Y, Kataoka K. 2003b. Novel cisplatin-incorporated polymeric micelles can eradicate solid tumors in mice. Cancer Res 63:8977–8983.

Nishiyama N, Iriyama A, Jang W-D, Miyata K, Itaka K, Inoue Y, Takahashi H, Yanagi Y, Tamaki Y, Koyama H, Kataoka K. 2005. Light-induced gene transfer from packaged DNA enveloped in a dendrimeric photosensitizer. Nat Mater 4:934–941.

Nishiyama N, Kataoka K. 2006. Nano-structured devices based on block copolymer assemblies for drug delivery: designing structures for enhanced drug function. Adv Polym Sci 193:67–101.

Niwa H, Yamamura K, Miyazaki J. 1991. Efficient selection for high-expression transfectants with a novel eukaryotic vector. Gene 108:193–199.

Ogris M, Wagner E. 2002. Targeting tumors with non-viral gene delivery systems. Drug Discov Today 7:479–485.

Oh DH, Stanley RJ, Lin M, Hoeffler WK, Boxer SG, Berns MW, Bauer E. 1997. Two-photon excitation of 4′-hydroxymethyl-4,5′,8-trimethylpsoralen. Photochem Photobiol 65:91–95.

Pack DW, Hoffman A, Pun S, Stayton PS. 2005. Design and development of polymers for gene delivery. Nat Rev Drug Discov 4:581–593.

Prasmickaite L, Høgset A, Berg K. 2001. Evaluation of different photosensitizers for use in photochemical gene transfection. Photochem Photobiol 73:388–395.

Stapert HR, Nishiyama N, Jiang D-L, Aida T, Kataoka K. 2000. Polyion complex micelles encapsulating light-harvesting ionic dendrimer zinc porphyrins. Langmuir 16:8182–8188.

Takakura Y, Hashida M. 1996. Macromolecular carrier systems for targeted drug delivery: Pharmacokinetic considerations on biodistribution. Pharm Res 13:820–831.

Wakebayashi D, Nishiyama N, Yamasaki Y, Itaka K, Kanayama N, Harada A, Nagasaki Y, Kataoka K. 2004. Lactose-conjugated polyion complex micelles incorporating plasmid DNA as a targetable gene vector system: Their preparation and gene transfecting efficiency against cultured HepG2 cells. J Control Release 95:653–664.

Available online at www.sciencedirect.com
SCIENCE DIRECT®
Journal of Controlled Release 113 (2006) 73–79
journal of controlled release
www.elsevier.com/locate/jconrel

Polyion complex micelles for photodynamic therapy: Incorporation of dendritic photosensitizer excitable at long wavelength relevant to improved tissue-penetrating property

Woo-Dong Jang [a,d,1], Yoshinori Nakagishi [c], Nobuhiro Nishiyama [b], Satoko Kawauchi [c], Yuji Morimoto [c], Makoto Kikuchi [c], Kazunori Kataoka [a,b,d,e,*]

[a] Department of Materials Engineering, Graduate School of Engineering, The University of Tokyo, 7-3-1 Hongo, Bunkyo-ku, Tokyo 113-8656, Japan
[b] Center for Disease Biology and Integrative Medicine, The University of Tokyo, 7-3-1 Hongo, Bunkyo-ku, Tokyo, 113-8656, Japan
[c] Department of Medical Engineering, National Defense Medical College, 3-2 Namiki, Tokorozawa, Saitama, 359-8513, Japan
[d] Core Research for Evolutional Science and Technology (CREST), Japan Science and Technology Agency (JST), Japan
[e] Center for NanoBio Integration, The University of Tokyo, 7-3-1 Hongo, Bunkyo-ku, Tokyo, 113-8656, Japan

Received 29 October 2005; accepted 10 March 2006
Available online 15 May 2006

Abstract

A polymeric micelle (DPcZn/m) system, which is formed via an electrostatic interaction of anionic dendrimer phthalocyanine (DPcZn) and poly(ethylene glycol)-poly(L-lysine) block copolymers (PEG-*b*-PLL), was prepared for use as an effective photosensitizer for photodynamic therapy. DPcZn/m exhibited strong Q band absorption around 650 nm, a useful wavelength for high tissue penetration. Dynamic light scattering studies indicated that the DPcZn/m system has a relevant size of 50 nm for intravenous administration. Under light irradiation, either DPcZn or DPcZn/m exhibited efficient consumption of dissolved oxygen in a medium to generate reactive oxygen species and an irradiation-time-dependent increase in photocytotoxicity. The photodynamic efficacy of the DPcZn was drastically improved by the incorporation into the polymeric micelles, typically exhibiting more than two orders of magnitude higher photocytotoxicity compared with the free DPcZn at 60-min photoirradiation.

Keywords: Dendrimer; Photosensitizer; Phthalocyanine; Polymeric micelle; Photodynamic therapy

1. Introduction

Photodynamic therapy is based on the accumulation of a photosensitizer in malignant tissue after its administration usually through intravenous route [1–5]. Subsequent illumination with laser light of an appropriate wavelength generates reactive oxygen species (ROS) which results in tissue destruction. For an effective photodynamic effect, several ideal properties of photosensitizers should be needed. From the chemical point of view, the materials should be pure and have a high quantum yield of singlet oxygen generation. From the biological point of view, it should have no dark toxicity and have high solubility in an aqueous medium for the easy administration. High tumor localization and long wavelength absorption are also very important for effective medical treatment.

In this context, we have recently reported ionic dendrimer porphyrin as an efficient photosensitizer for photodynamic therapy [6–9]. To obtain high quantum yields and effective energy absorption, photosensitizers must generally have large π-conjugation domains. Therefore, most of photosensitizers easily form aggregates, which provide a self-quenching effect of the excited state in aqueous medium due to their π–π interaction and hydrophobic characteristics [10,11]. To overcome these problems, the structure of ionic dendrimer porphyrin is promising, because the substitution of large dendritic wedges

* Corresponding author. Department of Materials Engineering, Graduate School of Engineering, The University of Tokyo, 7-3-1 Hongo, Bunkyo-ku, Tokyo 113-8656, Japan. Tel.: +81 3 5841 7138; fax: +81 3 5841 7139.
E-mail address: kataoka@bmw.t.u-tokyo.ac.jp (K. Kataoka).
[1] Current address: Department of Chemistry, Collage of Science, Yonsei University, 134 Sinchondong, Seodaemun-gu, Seoul 120-749, Korea.

0168-3659/$ - see front matter © 2006 Elsevier B.V. All rights reserved.
doi:10.1016/j.jconrel.2006.03.009

sufficiently prevents the formation of aggregates and provides high solubility in the aqueous medium. Furthermore, a charged ion surface can form polyion complex micelles by means of electrostatic interaction with an oppositely charged block copolymer. These types of polyion complex micelles [12] with a PEG shell were demonstrated to accumulate effectively and specifically in solid tumor tissue due to the hyperpermeability of tumor capillaries. However, the dendrimer porphyrin has a relatively short wavelength absorption, where the absorption maximum is 430 nm, which is a limitation to improvement for practical PDT application. In relation to this fact, several phthalocyanine molecules, including the one with a dendritic architecture, are of interest as a potential photosensitizer with appropriate wavelength absorption for practical PDT application [13–16]. Herein, we report the first example of dendritic phthalocyanine-incorporated polyion complex micelle formation and demonstrate an order-of-magnitude enhancement in photodynamic efficacy of the phthalocyanine dendrimer through the micelle encapsulation at an excitation wavelength with clinical relevance (~600 nm).

2. Materials and methods

2.1. Materials

N^{ε}-Z-L-lysine and bis(trichloromethyl) carbonate (triphosgene), for the synthesis of polyethylene glycol-block-poly-L-lysine (PEG-*b*-PLL), were purchased from Tokyo Kasei Co., Ltd. α-Methoxy-ω-amino-poly(ethylene glycol) (MeO-PEG-NH_2, Mw=12 kg/mol) was a kind gift from Nippon Oil and Fats Co., Ltd. Chemicals for dendrimer synthesis were purchased from Tokyo Kasei Co., Ltd. or Aldrich Chemical Co., Ltd. Tetrahydrofuran and hexane, used as a solvent for the synthetic reactions, were distilled from sodium benzophenone ketyl under Ar just before use. *n*-Pentanol and 1,8-diazabicyclo-(5,4,0)-undec-7-ene (DBU) for phthalocyanine dendrimer synthesis, were used as received without further purification.

2.2. Synthesis of block copolymer

MeO-PEG-NH_2 was precipitated in diethylether from chloroform, dried under reduced pressure and subsequently freeze-dried from benzene prior to use in the block copolymer synthesis. PEG-*b*-PLL was synthesized by a previously reported procedure [17]. Briefly, the *N*-carboxy anhydride of N^{ε}-Z-L-lysine was polymerized by initiation with CH_3O-PEG-NH_2 (12000 g/mol) in DMF under Ar, followed by deprotection of the Z group. GPC measurement of PEG-*b*-PLL exhibited single sharp peak at Mw of 16,600 and Mn of 16,300 based on PEG standards. From the ^1H NMR measurement in D_2O, the polymerization degree of the PLL segment was determined to be 39.

2.3. Synthesis of dendrimer phthalocyanine

Dendrimer phthalocyanine (DPcZn) was prepared from dimethyl-5-hydroxyisophthalate and 4-nitrophthalonitrile according to the literature method (Scheme 1) [15]. Briefly, the hydroxy group of dimethyl-5-hydroxyisophthalate (**1**) was protected with a tert-butyldiphenylsilyl chloride to obtain 3-*tert*-butyldiphenylsilyloxy-dimethylisophthalate (**2**), and then the methyl ester groups were reduced to obtain 3-*tert*-butyldiphenylsilyloxy-5-hydroxymethyl benzyl alcohol (**3**), which was reacted with **1** using Mitsunobu's coupling reaction to obtain a silyl-protected G1 dendron (**4**). G1 dendron with phenol core (**5**) was obtained from **4** by deprotection reaction using tetrabutylammonium fluoride (TBAF). A silyl-protected G2 dendron (**6**) was synthesized from **5** by Mitsunobu's coupling reaction, and then deprotected to obtain G2 dendron with phenol core (**7**). The alkali mediated coupling reaction of **6** with 4-nitrophthalonitrile gave phthalonitrile-cored G2 dendron (**8**). A mixture of **8** and Zn $(OAc)_2$ in *n*-pentanol was heated at 90 °C, and then a few drops of 1,8-diazabicyclo[5,4,0]undec-7-ene (DBU) were added. The mixture was refluxed with stirring overnight. The reaction mixture was chromatographed with silica gel to obtain DPcZn.

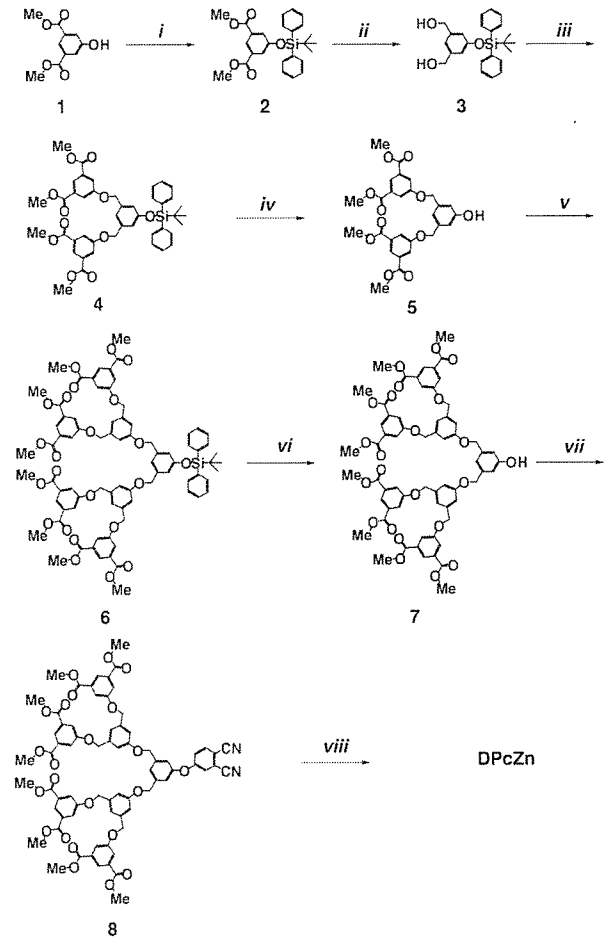

Scheme 1. Synthesis of phthalocyanine dendrimer. Reagents and conditions; (i) *tert*-butyldiphenylsilylchloride, imidazole, in DMF at 0 °C for 12 h; (ii) $LiAlH_4$ in THF at 0 °C for 12 h; (iii) **1**, diethylazodicarboxylate (DEAD), PPh3 in THF at 0 °C 12 h; (iv) tetrabutylammoniumfluoride (TBAF) in THF at 0 °C for 1 h; (v) **1**, DEAD, PPh3 in THF at 0 °C 12 h; (vi) TBAF in THF at 0 °C for 1 h; (vii) K_2CO_3, 4-nitrophthalonitrile, 18-crown in DMF at 60 °C for 12 h; (viii) Zn $(OAc)_2$, DBU in Pentanol reflux for 24 h.

2: yield 95%, ^{1}H NMR δ 8.18 (m, 1H, Ar–*H* in phthalate), 7.70 (m, 4H, *o-H* in C_6H_5), 7.57 (m, 2H, Ar–*H* in phthalate), 7.40 (m, 6H, *m,p-H* in C_6H_5), 3.86 (s, 6H, $-OCH_3$), 1.13 (s, 9H, $-C(CH_3)_3$). **3**: yield 89%, ^{1}H NMR δ 7.64 (m, 4H, *o-H* in C_6H_5), 7.32 (m, 6H, *m,p-H* in C_6H_5), 6.80 (m, 1H, Ar–*H* in C_6H_3), 6.58 (m, 2H, Ar–*H* in C_6H_3), 4.41 (s, 4H, $-CH_2-$), 1.03 (s, 9H, $-C(CH_3)_3$). **4**: yield 64%, ^{1}H NMR δ 8.27 (s, 2H, Ar–*H* in outer C_6H_3), 7.73 (s, 4H, Ar–*H* in outer C_6H_3), 7.69 (m, 4H, *o-H* in C_6H_5), 7.40 (m, 6H, *m,p-H* in C_6H_5), 7.02 (s, 1H, Ar–*H* in inner C_6H_3), 6.58 (s, 2H, Ar–*H* in inner C_6H_3), 4.97 (s, 4H, $-CH_2-$), 3.94 (s, 12H, $-CH_3$), 1.01 (s, 9H, $-C(CH_3)_3$). **5**: yield 90%, ^{1}H NMR δ 8.27 (s, 2H, Ar–*H* in outer C_6H_3), 7.80 (d, 4H, Ar–*H* in outer C_6H_3), 7.05 (s, 1H, Ar–*H* in inner C_6H_3), 6.92 (s, 2H, Ar–*H* in inner C_6H_3), 6.13 (s, 1H, –*OH*), 5.08 (s, 4H, $-CH_2-$), 3.94 (s, 12H, $-CH_3$). **6**: yield 79%, ^{1}H NMR δ 8.26 (s, 4H, Ar–*H* in outer C_6H_3), 7.79 (s, 8H, Ar–*H* in outer C_6H_3), 7.69 (m, 4H, *o-H* in $-C_6H_5$), 7.35 (m, 6H, *m,p-H* in $-C_6H_5$), 7.04 (s, 2H, Ar–*H* in inner C_6H_3), 6.98 (s, 1H, Ar–*H* in inner C_6H_3), 6.94 (s, 4H, Ar–*H* in mid C_6H_3), 6.81 (s, 2H, Ar–*H* in mid C_6H_3) 5.10 (s, 8H, outer $-CH_2-$), 5.00 (s, 4H, inner $-CH_2-$), 3.93 (s, 24H, $-CH_3$), 1.08 (s, 9H, $-C(CH_3)_3$). **7**: yield 91%, ^{1}H NMR δ 8.27 (s, 4H, Ar–*H* in outer C_6H_3), 7.79 (s, 8H, Ar–*H* in outer C_6H_3), 7.36 (s, 2H, Ar–*H* in inner C_6H_3), 7.08 (s, 1H, Ar–*H* in inner C_6H_3), 7.01 (s, 4H, Ar–*H* in mid C_6H_3), 6.87 (s, 2H, Ar–*H* in mid C_6H_3), 6.37 (s, 1H, –*OH*), 5.11 (s, 8H, outer $-CH_2-$), 5.09 (s, 4H, inner $-CH_2-$) 3.93 (s, 24H, $-CH_3$). **8**: yield 90%, ^{1}H NMR δ 8.28 (s, 4H, Ar–*H* in outer C_6H_3), 7.80 (s, 8H, Ar–*H* in outer C_6H_3), 7.68 (d, 1H, Ar–*H* in phthalonitrile), 7.45 (s 1H, Ar–*H* in inner C_6H_3) 7.28–7.23 (m, 2H, Ar–*H* in phthalonitrile), 7.15 (s, 2H, Ar–*H* in inner C_6H_3), 7.14 (s, 2H, Ar–*H* in mid C_6H_3), 7.04 (s, 4H, Ar–*H* in mid C_6H_3), 5.16 (s, 4H, outer $-CH_2-$), 5.13 (s, 8H, inner $-CH_2-$) 3.93 (s, 24H, $-CH_3$). DPcZn: yield 32%, ^{1}H NMR δ 9.22–8.88 (m, 8H, Ar–*H*), 8.2–7.7 (m, 28H, Ar–*H*), 7.6–6.9 (m, 60H, Ar–*H*), 5.2–4.9 (m, 48H, $ArOCH_2-$), 4.2–4.0 (m, 64H, $-CO_2CH_2-$), 1.7–1.1 (m, 256H, $-CH_2-$), 0.9–0.7 (m, 96H, $-CH_3$), MALDI-TOF-MS for $C_{416}H_{496}N_8O_{92}Zn$ *m/z*: calcd.: 7139 [M^+]; found 7150.

2.4. Preparation of polyion complex micelle

Polyion complex micelles were made from charged DPcZn with PEG-*b*-PLL. In a typical procedure, the PEG-*b*-PLL was dissolved in an aqueous NaH_2PO_4 solution and added to an aqueous solution of DPcZn in Na_2HPO_4 to give a solution containing polyion complex micelles. The ratio of positive charge to negative charge was fixed at 1:1.

2.5. Measurements

The DLS measurements were performed using a Photal dynamic laser scattering DLS-7000 spectrometer (Otsuka Electronics Co., Ltd., Osaka, Japan) equipped with GLG3050 488 nm Ar laser (NEC Co., Ltd., Japan) and/or Zetasizer Nano ZS-90 (Malvern Co., Ltd., USA) with 532 nm laser irradiation. The UV–Vis and fluorescence spectra were measured using a V-550 spectrophotometer (JASCO, Tokyo, Japan) and Type 850 spectrofluorometer (Hitachi, Tokyo, Japan), respectively. MALDI-TOF-MS was performed on a Bruker model Protein TOF mass spectrometer with dithranol as the matrix. ^{1}H NMR spectroscopy was performed in $CDCl_3$ or D_2O on a JEOL GSX-270 spectrometer operating at 270 MHz. GPC was performed with TOSOH HLC-8220 equipped with TSK-gel G4000HHR and G3000HHR column (eluent: DMF + 10 mM LiCl, temperature: 40 °C, detector: RI).

2.6. Oxygen consuming measurement

The oxygen consumption amount was measured using a Clark-type oxygen microelectrode with a tip diameter of 200 μm (PO_2-100DW, Eikou Kagaku Co., Ltd., Tokyo, Japan). The microelectrode was inserted into the PBS, which contained 3.13 μM of DPcZn or DPcZn/m and 10% FBS as a singlet oxygen acceptor, so that the tip was 100 μm above the bottom of the solution. Semiconductor laser light (660 nm; FWHM 6 nm, 25 mW/cm^2) was used for light irradiation. The solution was static and exposed to the atmosphere. Before each measurement, the system was calibrated in saline bubbled with air, in which the partial oxygen pressure was assumed to be 150 mm Hg.

2.7. Cell culture

HeLa cells were used in the cell culture studies. In the cytotoxicity assay, different concentration of DPcZn or DPcZn/m in Dulbecco's modified Eagle's medium (DMEM + 10% FBS) were added to cells in 96-wll culture plates (n=4). After a 24 h incubation at 37 °C, the photosensitizers were removed, and then plates were photoirradiated for 15–60 min with broad-band visible light using a halogen lamp (150 W) equipped with a filter passing light of 400–700 nm (fluence energy; 27–107 kJ/m^2). The viability of the cells was evaluated using mitochondrial respiration via the 3-(4,5-dimethyl thiazole-2-yl)-2,5-diphenyltetrazolium bromide cleavage assay (MTT assay) following incubation for 48 h after photoirradiation or removing the photosensitizers by washing in the case of the dark toxicity investigation.

2.8. Cellular uptake amount

After incubation of HeLa cells with 10 μM of DPcZn or DPcZn/m for 24 h in 60-mm dishes, the cells were washed three times with PBS, and then dissolved in 20% SDS solutions for 24 h to give a homogenous solution. As a control experiment, HeLa cells were incubated without DPcZn or DPcZn/m addition and then dissolved in 20% SDS solutions include fixed amount of DPcZn or DPcZn/m. The homogeneous solution thus obtained was put into a quartz cell to measure fluorescence. Before measuring samples, it was confirmed that DPcZn or DPcZn/m has comparable intensity of fluorescence in the 20% SDS solution. Quantitative analysis of uptake amount of DPcZn and DPcZn/m by HeLa cells was performed on a fluorescence spectrophotometer (Type 850, Hitachi, Tokyo, Japan). The excitation wavelength was 630 nm, and the emission wavelength was measured from 650 to 900 nm. The number of HeLa cells was 60,000.

3. Results and discussion

3.1. Synthesis of dendrimer phthalocyanine and preparation of polyion complex micelle

The synthesis of the ionic dendrimer phthalocyanine was accomplished by the method of Ng's group [15]. The second generation of dendritic phenol was reacted with 4-nitrophthalonitrile by an alkali-mediated coupling reaction to obtain the corresponding dendritic phthalonitrile, which was then treated with $Zn(OAc)_2$ and DBU in *n*-pentanol to give dendrimer phthalocyanine. Each step of synthesis was characterized by MALDI-TOF-MS and ^1H NMR measurement, and reaction yields were almost comparable to the literature. The dendrimer phthalocyanine thus obtained was treated with a THF/H_2O mixture solution of NaOH to obtain ionic dendrimer phthalocyanine (DPcZn; Fig. 1). DPcZn exhibited significantly high solubility at various pHs of the aqueous medium (over pH 4.3).

A cationic block copolymer (poly(ethyleneglycol)-*block*-poly-L-lysine: PEG-*b*-PLL; Fig. 1) was synthesized by the polymerization of the *N*-carboxy anhydride of N^{ε}-Z-L-lysine, initiated by ω-aminated poly(ethyleneglycol) (CH_3O-PEG-NH_2:12,000 g/mol) in DMF, followed by deprotection of the Z group according to a previously reported method [17]. The degree of polymerization was determined to be 39, which was confirmed by ^1H NMR. GPC measurement exhibited single sharp peak and relatively small molecular weight value compare to ^1H NMR result because of the interaction between PLL segment and GPC column.

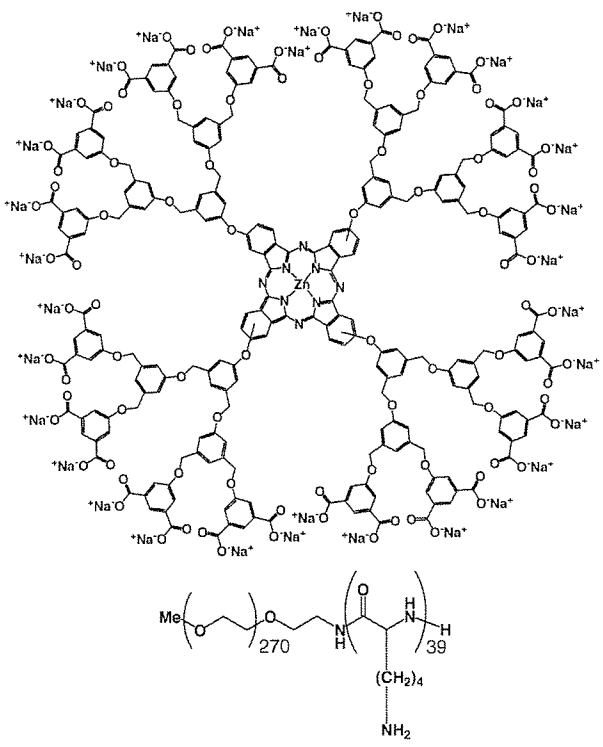

Fig. 1. Structures of DPcZn and PEG-*b*-PLL.

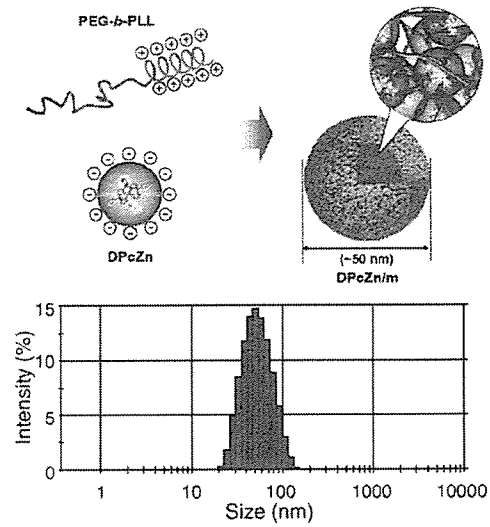

Fig. 2. Formation and DLS histogram analysis of polyion complex micelle (DPcZn/m).

Polyion complex micelles were prepared from negatively charged DPcZn with oppositely charged PEG-*b*-PLL. In a typical procedure, the PEG-*b*-PLL (14.2 mg) was dissolved in an aqueous NaH_2PO_4 (10 mM, 6.15 mL) and added to a solution of DPcZn (5 mg) in aqueous Na_2HPO_4 (10 mM, 13.85 mL) to give a solution containing polyion complex micelles encapsulating ionic DPcZn (Fig. 2). The ratio of positive charge to negative charge was fixed at 1:1. After mixing the two solutions, the pH of the solution becomes 7.3 (10 mM PBS). The resulting micelle has a diameter of ca. 50 nm with a narrow size distribution (unimodal, $\mu^2/\Gamma^2=0.12$), determined by a dynamic light scattering measurement (Zetasizer Nano ZS-90, Malvern Co., Ltd., USA) (Fig. 2). Furthermore, the diffusion coefficient of the resulting micelle was independent of the detection angle of the DLS measurement, suggesting that the polyion complex micelle of DPcZn with PEG-*b*-PLL is a narrowly dispersed spherical assembly.

3.2. Electronic absorption of dendrimer and micelle

Electronic absorption spectra of the dendrimer and micelle were measured (Fig. 3). DPcZn exhibits B band absorption at

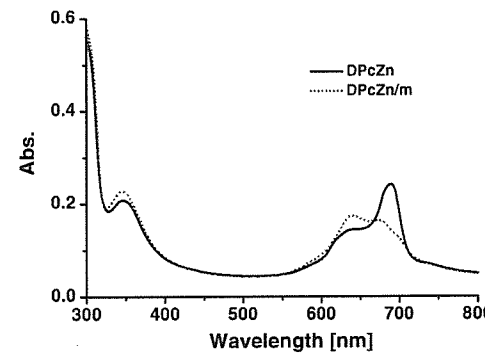

Fig. 3. Electronic absorption of DPcZn (15.3 μM) and DPcZn/m (15.3 μM) in 10 mM PBS.

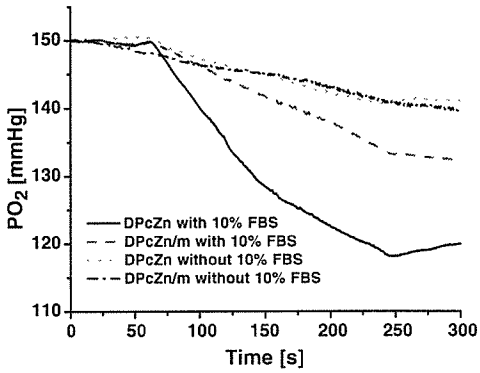

Fig. 4. Experimental setup for the measurement of oxygen consumption and the results obtained.

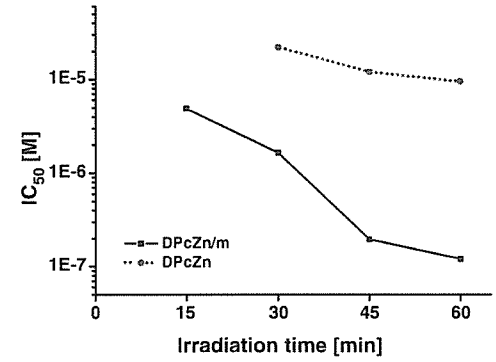

Fig. 6. Photoirradiation-time-dependent IC50 changes of DPcZn/m and DPcZn against HeLa Cells.

350 nm and strong Q band absorption at 685 nm, indicating successful dispersion as a monomeric species in the aqueous solution [16]. According to the formation of the polyion complex micelle, the absorption maximum of Q band absorption was slightly changed to 630 nm, indicating the possibility of slight aggregate formation of the core phthalocyanine units. Also, fluorescent intensity of DPcZn was drastically decreased by inclusion into the micelle (date not shown). The relatively small dendritic wedges may not perfectly prevent the aggregate formation of the phthalocyanine core units especially in the densely packed micellar core. Note that DPcZn (Mw=4901) is smaller than that of previously reported ionic dendrimer porphyrin (Mw=8029).

The absorption of light by tissue increases as the wavelength decreases and that the most efficient photosensitizers are those that have strong absorption bands between 600 and 800 nm. Therefore, although the relatively small dendritic wedges may not perfectly prevent collisional quenching, DPcZn has the potential for use as an effective photosensitizer in photodynamic therapy.

3.3. Oxygen consumption ability of the dendrimer phthalocyanine and micelle

The oxygen consumption amount was measured to evaluate ROS generation under photoirradiation [18]. Note that the DPcZn/m was sufficiently stable in the 10 mM PBS with 10% FBS, where the size and polydispersity of DPcZn/m in the 10 mM PBS with 10% FBS were almost comparable to those without FBS (data not shown). The oxygen partial pressure (PO_2) of DPcZn solution is significantly reduced by the irradiation of laser light (660 nm; FWHM 6 nm, 25 mW/cm^2) (Fig. 4). Although the consumption ability of DPcZn/m was lower than that of DPcZn, the PO_2 of DPcZn/m solution was also effectively reduced, indicating that either DPcZn or DPcZn/m can take part in the photochemical reaction to generate ROS. On the other hand, either DPcZn or DPcZn/m solution without 10%

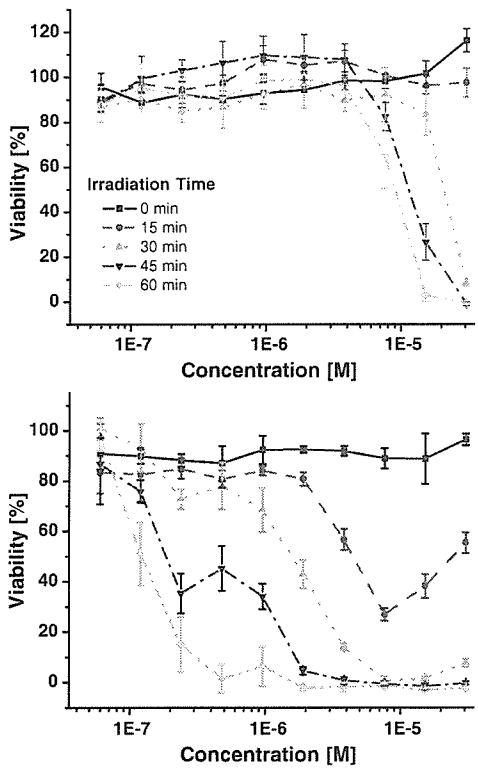

Fig. 5. Photocytotoxic profiles of DPcZn (top) and DPcZn/m (bottom) against HeLa cells.

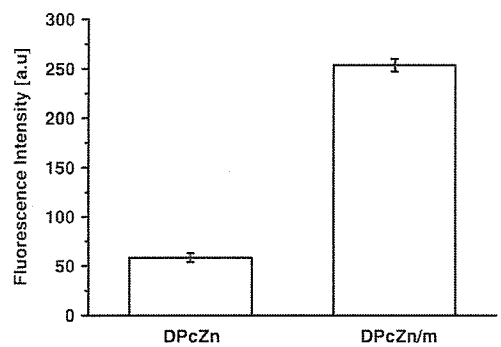

Fig. 7. Relative fluorescence intensities of uptaken DPcZn and DPcZn/m into HeLa cells. 10 μM of DPcZn or DPcZn/m was incubated with HeLa cells for 24 h. The excitation wavelength was 630 nm, and the fluorescence intensity was recorded from 650 to 900 nm.

FBS shows almost negligible change in the PO_2 upon the photoirradiation, indicating that the proteins in FBS act as sacrificial acceptors of ROS. In other words, if proteins do not exist in the medium, once generated, ROS promptly revert to oxygen molecules because of their short lifetimes.

3.4. Cytotoxicity of dendrimer phthalocyanine and micelle

The cytotoxicity of phthalocyanine dendrimer was assessed against HeLa cells (Fig. 5). The viability of cells upon photoirradiation was evaluated by MTT assay and determined to be a function of concentration and photoirradiation time with DPcZn and its micelle. DPcZn and DPcZn/m were incubated with the cells for 24 h and then fully washed with PBS to remove non-associated photosensitizers prior to photoirradiation. Under dark conditions, toxicities of DPcZn and DPcZn/m were negligible. However, either DPcZn or DPcZn/m exhibited photoinduced cytotoxicity upon the photoirradiation, where the cells were photoirradiated for 15–60 min with broad-band visible light using a halogen lamp (150 W) equipped with a filter passing light of 400–700 nm (fluence energy: 27–107 kJ/m^2). According to the exposure time increase, either DPcZn or DPcZn/m exhibited an increase in photocytotoxicity (Fig. 5). Very interestingly, the aspect of the photocytotoxicity increase is significantly different between DPcZn and DPcZn/m. As shown in Fig. 6, DPcZn exhibits a relatively small time-dependency, whereas DPcZn/m exhibits a remarkable change in the cell viability depending on the photoirradiation time. Typically at 60-min photoirradiation, DPcZn/m exhibited almost 100 times higher photocytotoxicity than free DPcZn. Although electronic absorption and oxygen consumption behaviours exhibited quenching signature, DPcZn/m have significantly high PDT efficacy compare to DPcZn alone. On the other hand, the cell viability exhibits abnormal increase with increase in the concentration of DPcZn/m at the 15-min light irradiation. There is various reasons can be considerable such as compositional change of micellar structure or microenvironment change around photosensitizers. To understand this phenomenon, we need further investigation.

In view of the negatively charged surface of mammalian cells, charge neutralization of DPcZn by formulation of micelle possibly improves the cellular uptake. In fact, DPcZn/m showed a 4 times higher cellular uptake compared to DPcZn alone when HeLa cells were incubated with 10 μM of DPcZn or DPcZn/m for 24 h (Fig. 7). Nevertheless, the enhancement of photocytotoxicity by the micelle formulation is much larger than the improvement in cellular uptake. Furthermore, this result is quite controversial to the quenching signature of DPcZn within the micellar core.

This phenomenon presumably suggests that the PEG shell layer of the DPcZn/m and micro environment around DPcZn may have a role in altering the intracellular mechanism of DPcZn to increase the photocytotoxicity. Also, in the case of DPcZn/m, a large amount of ROS can be generated at once within the micellar core. Therefore, the higher local concentration of ROS around the micelle may easily exceed the threshold of photodamage against typical cellular organelles.

The remarkably enhanced photocytotoxicity of the micellar system may be very advantageous point for practical applications. Because the most of photosensitizers have large π-conjugation domain and hydrophobic skeleton, photosensitizers easily form aggregates within the highly concentrated micellar core via π–π and hydrophobic interactions. The formation of aggregates result in the collisional quenching of the excitation state, photocytotoxicity will be impaired when the micellar structure occurs [19]. In contrast, because DPcZn shows less collisional quenching by micelle formation due to the large dendritic wedges, photocytotoxicity will be maintained, or even enhanced in the micelle form. The DPc-incorporated micelle is assumed to gradually dissociate into the constituent DPc and block copolymer in the body by dilution; therefore, eventually long-term phototoxicity due to non-specific uptake of photosensitizers in normal tissue may be avoidable after PDT using this micelle system [20]. Actually, our recent experiment showed that the dendritic photosensitizers have almost no skin toxicity under light irradiation compared to the clinically used photosensitizer formulation Photofrin® [21,22].

4. Conclusions

The first example of polyion complex micelle formation of DPcZn and its photodynamic efficacy were demonstrated. DPcZn/m exhibited long wavelength absorption around 650 nm, which is very advantageous for the treatment of deep lesions, because the long wavelength light is less absorbed by melanin dyes in skin tissue or heme proteins in blood. Furthermore, the micellar formulation may improve the longevity in blood circulation that achieves cumulative accumulation in the lesion with hyperpermeability, such as a macular degeneration [23], due to the enhanced permeation and retention (EPR) effect [24]. The in vivo PDT efficacy of DPcZn/m is now under investigation in our research group using disease models, such as cancer and macular degeneration.

Acknowledgement

This study was supported by Industrial Technology Research Grant Program in 2004 from New Energy and Industrial Technology Development Organization (NEDO) of Japan.

References

[1] R.K. Pandey, G. Zhang, in: K.M. Kadish, K.M. Smith, R. Guilard (Eds.), Porphyrin Handbook, vol. 6, Academic press, New York, 2000, pp. 157–230.
[2] I.J. Macdonald, T.J. Dougherty, Basic principles of photodynamic therapy, J. Porphyr. Phthalocyanines 5 (2) (2001) 105–129.
[3] Y. Takeuchi, K. Ichikawa, S. Yonezawa, K. Kurohane, T. Koishi, M. Nango, Y. Namba, N. Oku, Intracellular target for photosensitization in cancer antiangiogenic photodynamic therapy mediated by polycation liposome, J. Control. Release 97 (2) (2004) 231–240.
[4] N. Merclin, T. Bramer, K. Edsman, Iontophoretic delivery of 5-aminolevulinic acid and its methyl ester using a carbopol gel as vehicle, J. Control. Release 98 (1) (2004) 57–65.
[5] Y.N. Konan-Kouakou, R. Boch, R. Gurny, E. Allemann, In vitro and in vivo activities of verteporfin-loaded nanoparticles, J. Control. Release 103 (1) (2005) 83–91.

[6] N. Tomioka, D. Takasu, T. Takahashi, T. Aida, Electrostatic assembly of dendrimer electrolytes: negatively and positively charged dendrimer porphyrins, Angew. Chem., Int. Ed. Engl. 37 (11) (1998) 1531–1534.
[7] N. Nishiyama, H.R. Stapert, G.D. Zhang, D. Takasu, D.L. Jiang, T. Nagano, T. Aida, K. Kataoka, Light-harvesting ionic dendrimer porphyrins as new photosensitizers for photodynamic therapy, Bioconjug. Chem. 14 (1) (2003) 58–66.
[8] H.R. Stapert, N. Nishiyama, D.L. Jiang, T. Aida, K. Kataoka, Polyion complex micelles encapsulating light-harvesting ionic dendrimer zinc porphyrins, Langmuir 16 (21) (2000) 8182–8188.
[9] W.-D. Jang, N. Nishiyama, G.-D. Zhang, A. Harada, D.-L. Jiang, S. Kawauci, Y. Morimoto, M. Kikuchi, H. Koyama, T. Aida, K. Kataoka, Supramolecular nanocarrier of anionic dendrimer porphyrins with cationic block copolymers modified with polyethylene glycol to enhance intracellular photodynamic efficacy, Angew. Chem., Int. Ed. Engl. 44 (3) (2005) 419–423.
[10] T. Sato, D.-L. Jiang, T. Aida, A blue-luminescent dendritic rod: poly (phenyleneethynylene) within a light-harvesting dendritic envelope, J. Am. Chem. Soc. 121 (45) (1999) 10658–10659.
[11] S.A. Gerhardt, J.W. Lewis, D.S. Kliger, J.Z. Zhang, U. Simonis, Effect of micelles on oxygen-quenching processes of triplet-state para-substituted tetraphenylporphyrin photosensitizers, J. Phys. Chem., A 107 (15) (2003) 2763–2767.
[12] Y. Kakizawa, K. Kataoka, Block copolymer micelles for delivery of gene and related compounds, Adv. Drug Deliv. Rev. 54 (2) (2002) 203–222.
[13] E.A. Lukyanets, Phthalocyanines as photosensitizers in the photodynamic therapy of cancer, J. Porphyr. Phthalocyanines 3 (6–7) (1999) 424–432.
[14] P.-C. Lo, J.-D. Huang, D.Y.Y. Cheng, E.Y.M. Chan, W.-P. Fong, W.-H. Ko, D.K.P. Ng, New amphiphilic silicon(IV) phthalocyanines as efficient photosensitizers for photodynamic therapy: synthesis, photophysical properties, and in vitro photodynamic activities, Chem. Eur. J. 10 (19) (2004) 4831–4838.
[15] A.C.H. Ng, X. Li, D.K.P. Ng, Synthesis and photophysical properties of nonaggregated phthalocyanines bearing dendritic substituents, Macromolecules 32 (16) (1999) 5292.
[16] Z. Sheng, X. Ye, Z. Zheng, S. Yu, D.K.P. Ng, T. Ngai, C. Wu, Transient absorption and fluorescence studies of disstacking phthalocyanine by poly (ethylene oxide), Macromolecules 35 (9) (2002) 3681–3685.
[17] A. Harada, K. Kataoka, Formation of polyion complex micelles in an aqueous milieu from a pair of oppositely-charged block copolymers with poly(ethylene glycol) segments, Macromolecules 28 (15) (1995) 5294–5299.
[18] S. Kawauchi, S. Sato, Y. Morimoto, M. Kikuchi, Correlation between oxygen consumption and photobleaching during in vitro photodynamic treatment with ATX-S10(Na(II) using pulsed light excitation: Dependence of pulse repetition rate and irradiation time, Photochem. Photobiol. 80 (2004) 216–223.
[19] W. Spiller, H. Kliesch, D. Wöhrle, S. Hackbarth, B. Röder, G. Schnurpfeil, Singlet oxygen quantum yields of different photosensitizers in polar solvents and micellar solutions, J. Porphyr. Phthalocyanines 2 (2) (1998) 145–158.
[20] S.B. Brown, E.A. Brown, I. Walker, The present and future role of photodynamic therapy in cancer treatment, Lancet Oncol. 5 (8) (2004) 497–508.
[21] Y. Nakagishi, Y. Morimoto, S. Kawauchi, W.-D. Jang, N. Nishiyama, Y. Ozeki, K. Kataoka, M. Kikuchi, Photodynamic therapy combined with drug delivery system using a macromolecular polymeric micelle, Abstracts of 96th Annual Meeting 2005-American Association for Cancer Research, Anahim, USA, April 16-20, 2005.
[22] R. Ideta, F. Tasaka, W.-D. Jang, N. Nishiyama, G.-D. Zhang, Aou. Harada, Y. Yanagi, Y. Tamaki, T. Aida, K. Kataoka, Nanotechnology-based photodynamic therapy for neovascular disease using a supramolecular nanocarrier loaded with a dendritic photosensitizer, Nano Lett. 5 (2005) 2426–2431.
[23] D.N. Zacks, E. Ezra, Y. Terada, N. Michaud, E. Connolly, E.S. Gragpidas, J.W. Miller, Verteporfin photodynamic therapy in the rat model of choroidal neovascularization: angiographic and histologic characterization, Invest. Ophthalmol. Vis. Sci. 43 (2002) 2384–2391.
[24] H. Maeda, J. Wu, T. Sawa, Y. Matsumura, K. Hori, Tumor vascular permeability and the EPR effect in macromolecular therapeutics: a review, J. Control. Release 65 (1–2) (2000) 271–284.

Development of a Fitting Model Suitable for the Isothermal Titration Calorimetric Curve of DNA with Cationic Ligands

Wankee Kim,[†] Yuichi Yamasaki,*[,†] and Kazunori Kataoka*[,†,‡]

Department of Materials Science and Engineering, School of Engineering, The University of Tokyo, 7-3-1 Hongo, Bunkyo-ku, Tokyo 113-8656, Japan, and Center for Disease Biology and Integrative Medicine, Graduate School of Medicine, The University of Tokyo, 7-3-1 Hongo, Bunkyo-ku, Tokyo 113-0033, Japan

Received: December 28, 2005; In Final Form: April 12, 2006

A novel curve fitting model was developed for the isothermal titration calorimetry (ITC) of a cationic ligand binding to DNA. The ligand binding often generates a DNA conformational change from an elongated random coil into a compact collapsed form that is referred to as "DNA condensation". The ligand binding can be classified into two regimes having different binding constants K_i, i.e., the binding to an elongated DNA chain with a binding constant K_1 and with K_2 that occurred during the conformational transition. The two-variable curve fitting models are usually bound by a strict regulation on the difference in the values of the binding constants $K_1 > K_2$. For the DNA condensation, however, the relationships for K_1 and K_2 are still unclear. The novel curve fitting model developed in this study takes into account this uncertainty on the relationship of the binding constants and is highly flexible for the two-variable binding constant system.

Introduction

Isothermal titration calorimetry (ITC) is a useful method to explore the interaction between DNA and cationic ligands.[1−10] By adding a solution of cationic ligands to a DNA solution, the ITC instrument measures the heat accompanied by the binding reaction. The thermodynamic parameters such as changes in enthalpy, entropy, and free energy can be obtained by fitting the ITC curve to an adequate curve fitting model. Nevertheless, general curve fitting models are useful only for simple binding systems, and they may not be applied to particular cases such as DNA condensation.

In general, there are three kinds of curve fitting models, i.e., the single set of identical sites (SSIS) model, two sets of independent sites (TSIS) model, and sequential binding sites (SBS) model.[11,12] The SSIS model satisfies many ligand binding systems when all the binding sites on the substance are identical. The following parameters, stoichiometry N, binding constant K, and change in enthalpy ΔH can be obtained using this fitting model. The TSIS model, which is useful when substances have two kinds of binding sites, enables us to calculate both sets of parameters N_1, K_1, ΔH_1 and N_2, K_2, ΔH_2 for the first and second ligand bindings. While the TSIS model seems to be well adapted to various cases, it should not be applied to the particular system where K_1 is smaller than K_2, because this model is constructed assuming that K_1 is larger than K_2. The SBS model is appropriate for the system, such as the binding of multiple ligands to transition metal ions, for example, the binding of four Br^- ions to Cd^{2+} leading to $CdBr_4^{2-}$. For this case, the number of sequential sites should be integral. The absence of a parameter equivalent to N indicates that the curve fitting is carried out by changing only two parameters, K and H, on each site.

Concerning the binding of cationic ligands to DNA, a conformational change in the DNA chain may affect their binding behavior. The DNA chain collapses after some fraction of negative charges on the phosphate backbone is neutralized by cationic ligands, which is referred to as DNA condensation. The binding process of cationic ligands to DNA can be classified into two parts, a simple binding without a DNA conformational transition and another binding event that followed during the conformational transition. The binding constant for the former is K_1 and that for the latter is K_2. During the beginning of ligand binding, the former binding process proceeds where the DNA chains retain their conformation. Consequently, the latter binding occurs after the former was completed, resulting from the DNA conformational transition.

This scheme is consistent with the prediction of the counterion condensation (CC) theory developed by Oosawa and Manning and with the experimental results obtained from electrophoresis.[13] The CC theory indicates the presence of critical residual charges on elongated DNA chains that results from the former ligand binding. While the degree of charge neutralization depends on the ligand concentration, the critical value of charge neutralization is determined by their valence. For example, the values of DNA in the presence of monovalent, divalent, and trivalent cations are 0.76, 0.88, and 0.92, respectively.[14] Bloomfield concluded that the DNA chains retain their conformation until the degree of charge neutralization is increased to 0.90, indicating that cationic ligands with their valence equal to or grater than 3 possesses the potential to generate DNA condensation. On the contrary, it was clarified that almost all of the negative charges are neutralized in the collapsed state.[15] These experimental results suggest that the DNA conformation and its residual charges correlate with each other, and that the binding manner of the cationic ligands is also affected by DNA conformation. Therefore, the binding classification described above is appropriate for the ligand binding to DNA phosphates.

* To whom correspondence should be addressed: Kazunori Kataoka, tel +81-3-5841-7138, fax +81-3-5841-7139, e-mail kataoka@bmw.t.u-tokyo.ac.jp; Yuichi Yamasaki, tel +81-3-5841-7145, fax +81-3-5841-7139, e-mail yamasaki@bmw.t.u-tokyo.ac.jp.

† Department of Materials Science and Engineering, School of Engineering, The University of Tokyo.

‡ Center for Disease Biology and Integrative Medicine, Graduate School of Medicine, The University of Tokyo.

10.1021/jp057554e CCC: $33.50
Published on Web 05/17/2006

To obtain thermodynamic parameters from the ITC measurements, the suitable fitting model should be carefully chosen by considering the relationship of the magnitude of the binding constants. For the DNA condensation, however, this relationship has so far been unknown. Recently, Teif and Lando theoretically pointed out that the DNA conformational change to the collapsed state takes place when $K_2 > K_1$.[16] Actually, Mel'nikov et al. reported the cooperative binding observed in the transition region of the DNA condensation induced by a cationic surfactant.[17] Thus, we developed a novel fitting model suitable for this situation $K_2 > K_1$ to analyze the binding isotherm obtained from the DNA condensation. In this paper, the binding isotherms obtained from the DNA condensation induced by a low molecular weight condensing reagent, cobalt hexamine ($Co(NH_3)_6^{3+}$), and by a polymeric cation poly(ethylene glycol)−poly(L-lysine) block copolymer (PEG−PLL), are demonstrated as typical examples. The former is treated as a standard chemical of a DNA condensation investigation[18] and the latter as a promising polycation as a gene carrier.[19] A comparison of both binding isotherms and the validity of the novel fitting model will be discussed in detail.

Experimental Section

Materials. The plasmid pGL3 DNA (5256 base pairs) was purchased from Promega (Madison, WI). The plasmid DNA (pDNA) was amplified in competent DH5α *Escherichia coli* and purified using the Qiafilter giga kit (QIAGEN, Germany). A stock solution of pDNA was prepared by dissolving purified pDNA in Millipore grade water containing 10 mM NaCl without any buffer solution. The DNA concentration was determined by the absorption at 260 nm. The PEG−PLL block copolymer with the average PEG molecular weight of 12 000 and the average degree of lysine polymerization of 109 was used in this study. The PEG−PLL block copolymer was prepared as already prescribed.[20] Let us now briefly explain the synthesis. PEG−PLL was synthesized using α-methoxy-ω-amino-PEG to initiate polymerization of the *N*-carboxy anhydride of the *Z*-protected lysine. The length of the lysine segment was regulated by the ratio of the monomer to PEG initiator. The deprotection of lysine was carried out under acidic conditions. ^{1}H NMR and size exclusion chromatography were employed for characterization of this block copolymer. The degree of polymerization is deduced by the ratio of the methylene proton of PEG to that on the lysine residue. Cobalt(III) hexamine trichloride was obtained from Wako Pure Chemicals (Osaka, Japan) and used as received.

Isothermal Titration Calorimetry. Isothermal titration calorimetry (ITC) was performed using a Microcal VP-ITC calorimeter (Northampton, MA) with the normal cell (1.4643 mL) at 30 °C. Two milliliters of pDNA solution (0.3 mM in phosphate) was poured inside the cell after three rinses with 10 mM NaCl solution. The condensing agents were titrated into the pDNA solutions using an injection syringe. The concentrations of cobalt hexamine and PEG−PLL were chosen to be 1.2 and 3 mM (in lysine unit), respectively. Each titration consisted of a preliminary 1-μL injection followed by 29 subsequent 10-μL injections at 3-min intervals. Control experiments were carried out for both ligands to determine the heats of ligand dilution, because the dilution effect should be subtracted to obtain the heat of binding. Prior to the ligand binding experiments, the calorimeter was verified by carrying out the Tris base protonation reaction with hydrochloric acid ($\Delta H = -13.58$ kcal/mol).

Analysis of ITC Curve. The analysis of the obtained ITC curves was performed using origin software with version 5.0 attached to the instrument. First, the integrated ITC curves were obtained from the raw data of the power change at each injection, using the add-on module for the purpose in the software, and then the fittings of those data to the fitting function developed here were performed to obtain the thermodynamic parameters, using a fitting tool prepared in the software, which was based on the Levenberg−Marquardt nonlinear fitting algorithm.

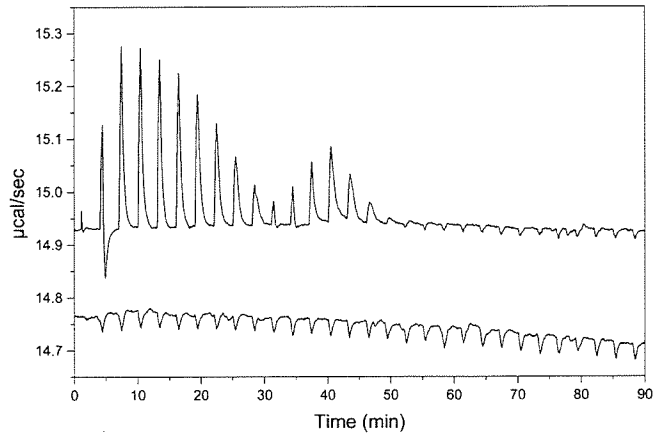

Figure 1. Raw data of ITC measurement for cobalt hexamine binding to plasmid pGL3 DNA in 10 mM NaCl aqueous solution. The upper curve shows the heats resulting from the titration of cobalt hexamine to pDNA solution. The lower curve was obtained by the titration without pDNA, indicating the heats generated by the dilution of the ligand solution. To obtain the ITC binding curves, the lower one should be subtracted from the upper one.

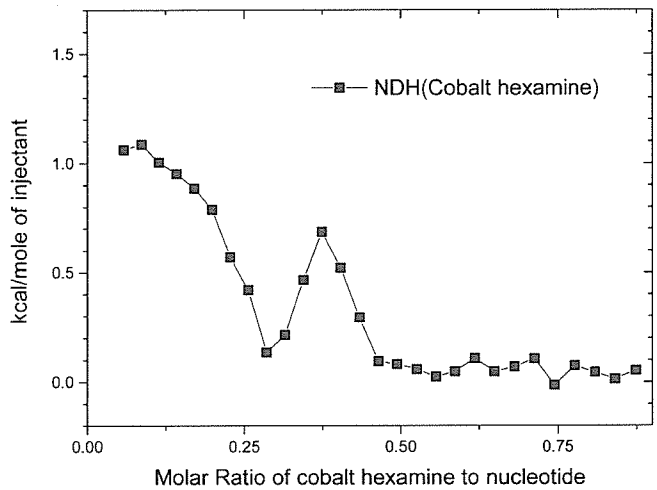

Figure 2. Integrated ITC curve of cobalt hexamine binding to plasmid pGL3 DNA in 10 mM NaCl aqueous solution. This ITC binding curve was calculated from both curves in Figure 1. Endothermic two-stage binding was observed during this ligand binding.

Results

Typical nonintegrated titration curves are shown in Figure 1. The upper curve was obtained by titrating pDNA with cobalt hexamine, and the lower curve was obtained without pDNA indicating the heat of the dilution of cobalt hexamine solution. The upper curve includes the heats resulting from both the dilution effect and the binding reaction. To obtain integrated binding curves as shown in Figure 2, the peaks of both curves were integrated and the latter was subtracted from the former. Figure 2 indicates that the binding of cobalt hexamine onto pDNA can be classified into two stages. Endothermic events were observed during both stages, suggesting that this binding

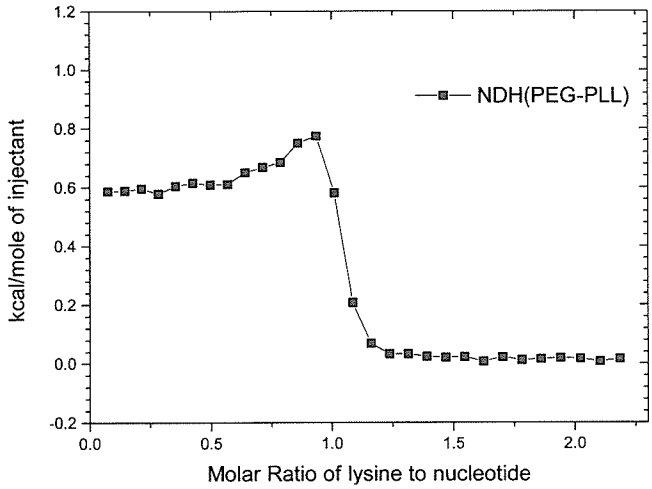

Figure 3. Integrated ITC curve of PEG−PLL binding to plasmid pGL3 DNA in water with 10 mM NaCl. The endothermic binding was completed by the charge ratio of 1.2.

was entropically driven. This result is in good agreement with those reported by other researchers.[2,4]

In this system, the initial binding stage was completed with the charge ratio of 0.9. The second stage was observed when a further addition of cobalt hexamine occurred. No heat was generated at the region in the charge ratio range higher than 1.5. From the results of turbidity measurement, a significant decrease in the transmittance resulting from the formation of aggregates was observed immediately following the second binding stage (data not shown). After the titration measurement, precipitates were visually observed in the sample solution.

The integrated ITC curve of the PEG−PLL binding to pDNA is shown in Figure 3, indicating an endothermic ligand binding the same as that observed in the $Co(NH_3)_6^{3+}$/pDNA system. Although the two-stage binding observed in the ITC curve of the cobalt hexamine titration is well separated, no segregation was observed in the ITC profile for the PEG−PLL/pDNA system. The PEG−PLL binding was completed with the charge ratio of 1.2.

Development of the Novel Fitting Model

A novel fitting model is based on the combination of the single set of identical sites (SSIS) model. Let us introduce the SSIS model as follows.[11,12] Generally, the binding constant K and the relationship of the total and free ligand concentrations (X_t and $[X]$) are represented by eqs 1 and 2, respectively

$$K = \frac{\Theta}{(1-\Theta)[X]} \quad (1)$$

$$X_t = [X] + N\Theta M_t \quad (2)$$

where N is the number of binding sites, M_t is the total concentration of macromolecule, and Θ is the fractional sites occupied by ligand. Combining eqs 1 and 2 gives eq 3

$$\Theta^2 - \Theta\left[1 + \frac{X_t}{NM_t} + \frac{1}{NKM_t}\right] + \frac{X_t}{NM_t} = 0 \quad (3)$$

The total heat content Q of the solution contained in the sample cell at fractional saturation Θ is

$$Q = N\Theta M_t \Delta H V_0 \quad (4)$$

where ΔH is the molar heat of ligand binding and V_0 is the cell

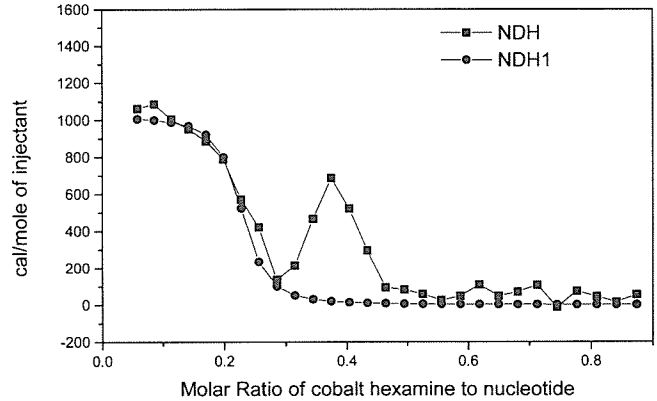

Figure 4. Integrated ITC curve of cobalt hexamine binding to plasmid pGL3 DNA (■) and representative ITC curve NDH1 generated from the SSIS model with the following fitting parameter (●). $N_1 = 0.216 \pm 0.004$, $K_1 = (17.79 \pm 4.99) \times 10^5\ M^{-1}$, $\Delta H_1 = 1019 \pm 30$ cal/mol.

volume. Solving the quadratic eq 3 for Θ and then substituting this into eq 4 gives eq 5

$$Q = \frac{NM_t\Delta HV_0}{2}[1 + (X_t/NM_t) + (1/NKM_t) - \sqrt{(1 + (X_t/NM_t) + (1/NKM_t))^2 - (4X_t/NM_t)}] \quad (5)$$

The value of Q can be calculated for any designated values of N, K, and ΔH at the end of the ith injection and designated $Q(i)$. The parameter of interest for comparison with the experiment, however, is the change in heat content from the completion of the $(i-1)$th injection to completion of the i-th injection. The expression for Q in eq 5 only applies to the liquid contained in volume V_0. Therefore, after an injection is completed, it is obvious that a correction must be made for the displaced volume (i.e., ΔV_i = injection volume) since some of the liquid in V_0 after the $(i-1)$th injection will no longer be in V_0 after the ith injection, even though it will contribute to the heat effect (assuming that the kinetics of the reaction and mixing are fast) before it passes out of the working volume V_0. The liquid in the displaced volume contributes about 50% as much heat effect as an equivalent volume remaining in V_0. The correct expression for the heat released $\Delta Q(i)$ from the ith injection is

$$\Delta Q(i) = Q(i) + \frac{dV_i}{V_0}\left[\frac{Q(i) + Q(i-1)}{2}\right] - Q(i-1) \quad (6)$$

By dividing $\Delta Q(i)$ with moles in the ith injected volume, the normalized heat, NDH(i), is obtained. Hereafter, NDH(i) is described by NDH(N, ΔH, K) because NDH(i) is dependent on the three parameters, N, ΔH and K.

A set of fitting parameters, N_1, K_1, and ΔH_1, is assigned to the initial binding stage of cationic ligands to the elongated pDNA, and another set, N_2, K_2, and ΔH_2, is assigned to the second binding stage during the pDNA conformational transition. On the basis of the SSIS model, the optimum fitting parameters for the initial stage provide the most suitable ITC curve as shown in Figure 4.

On comparison of the ITC curves for the PEG−PLL/pDNA system with that for $Co(NH_3)_6^{3+}$/pDNA, the molar ratios where the second binding stage appeared disagree. It is assumed that the second binding stage in the PEG−PLL system is immediately generated after the initial binding stage. In the system of cobalt hexamine, however, the generation of the second stage requires an excess amount of ligand in the bulk solution, corresponding to the delay of the second stage in Figure 2. As

shown in Figure 3, the second stage in the PEG−PLL system was almost finished around the charge equivalent condition. Therefore, both the initial and second binding stages in the PEG−PLL system coexist in a certain region where the molar ratio is greater than 0.5. This binding feature agrees with the results obtained from the direct observation of the DNA condensation using fluorescence microscopy.[21]

On the contrary, the two binding stages were well separated in the system of cobalt hexamine. In this system, the second binding stage during the DNA conformational change occurs after the initial stage where the fraction of the bound ligand reaches the critical one and all of the injected cationic ligands are consumed in the initial binding stage. As the injections of the cationic ligands are repeated, the amount of bound ligands gradually increases and reaches a maximum value at the molar ratio of 0.3, corresponding to the critical residual charges of the elongated DNA double helices, i.e., the end point of the initial binding stage. Under this condition, the added ligands do not tend to bind the elongated DNA, then the heat generated by the binding gradually decreases. The further addition of cationic ligands induces the DNA conformational change or "DNA condensation". During this transition, the second binding stage of the cationic ligands is promoted. The presence or absence of the delay between the two binding stages seems to be a significant phenomenological difference. Therefore, the effect of this delay is taken into consideration in the novel fitting model developed in this study.

Prior to describing the delay of the second binding stage observed in the $Co(NH_3)_6^{3+}$/pDNA system, the curve fitting for the second binding stage should be discussed here. On the basis of the SSIS model, a general ITC curve should be produced as a decreased sigmoidal curve as shown in Figure 4 (NDH1). According to the results of the DNA conformational analysis under fluorescence microscopy, both the elongated and collapsed DNA chains coexist during the transition region of the DNA condensation.[22] Thus, the population of collapsed DNAs should gradually increase with an increase in the molar ratio. This leads to the decrease in the fraction of ligands bound to the elongated DNA and the increase in that of the collapsed one. If the delay in the second binding stage was missing, the residual ligands not involved in the initial binding stage ideally contribute to the second binding stage. The amount of this residual ligand is represented by differences between the maximum and each fraction of the binding ligand, which can be expressed by an increased sigmoidal curve. Because the sigmoidal NDH having N, K, ΔH as a variable is linearly dependent on the fraction of ligands (Θ), Θ can be described as the absolute value of NDH divided by ΔH, ABS(NDH/ΔH).

To describe the fraction of the occupied site on DNA during the second binding stage, an NDH3 sigmoidal curve was employed. The definition of parameters for NDH3 is basically the same as those for the NDH1, but only N_3 is variable when considering the delay of the second binding stage. When N_3 is equal to N_1, the initial binding stage is immediately followed by the second binding stage during the DNA condensation. On the contrary, as N_3 becomes larger than N_1, the second binding stage is separated from the initial binding stage, indicating that the delay in the second stage is significant in the ITC curve. Thus, the fraction of the occupied site on DNA during the second stage is represented by ABS((ΔH_1 − NDH3)/ΔH_1) in Figure 5, which is derived from 1 − ABS(NDH3/ΔH_1). We intend to generate for the second binding stage the NDH2 curve which is a function of N_2, K_2, and ΔH_2. The second binding stage of the ITC curve was fitted by the product of the

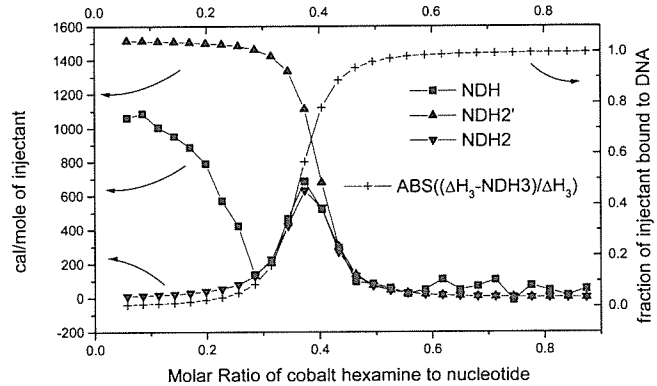

Figure 5. Representative curve for the second binding stage during pDNA condensation (NDH2; ▼).

hypothetical ITC curve NDH2′ and the increased sigmoidal curve ABS((ΔH_1 − NDH3)/ΔH_1). The ITC curve NDH2′ that corresponds to a standard ITC curve with the absence of the initial binding stage is generated by the SSIS model, indicating that the NDH2′ curve is defined by N_2', K_2', and $\Delta H_2'$. The product was defined as NDH2 where N_2' − N_3 (the difference of N_2' and N_3), K_2', and $\Delta H_2'$ are selected for N_2, K_2, and ΔH_2, respectively.

Application of New Model

The optimum fittings for the experimental ITC curves of both $Co(NH_3)_6^{3+}$/pDNA and PEG−PLL/pDNA are shown in Figures 6 and 7, respectively. The ITC curves were fitted by the sum of NDH1 and NDH2, corresponding to the initial and second binding stages, respectively. The sum of these two curves represents the relation of the total heats accompanied by ligand binding on DNA to the mixing ratio. Although the curve NDH1 is defined by the set of three parameters, N_1, K_1, and ΔH_1, another curve, NDH2, was defined by the set of six parameters, N_3, K_1, ΔH_1, N_2', K_2', and $\Delta H_2'$. In this method, both curves, NDH1 and NDH2, were simultaneously fitted. The difference in N_2' and N_3, which is described by N_2, means the binding stoichiometry for the second binding stage in the novel fitting model, and the difference in N_1 and N_3 reflects the delay of the second binding stage. The important thermodynamic parameters are listed in Tables 1 and 2. For both the simplified notation and comparison with the reported data, the binding stoichiometry for the second binding stage is represented by the parameter N_2 in the tables.

Discussion

The cooperative binding of polycations to DNA chains has been discussed as a typical binding feature of polyelectrolytes. Similar binding processes have already been independently considered by McGhee and von Hippel[23] and by Schwarz.[24] MaGhee and von Hippel suggested the concept of cooperativity of protein binding to DNA using the following three binding modes: (1) the binding to the isolated site with an intrinsic binding constant K, (2) a singly contiguous site to which a linear polymer binds with binding constant $K\omega$, and (3) a doubly contiguous site to which a linear polymer binds with binding constant $K\omega^2$, where ω is the cooperativity constant. When $\omega > 1$, the cationic ligands attract each other and the binding is positively cooperative; when $\omega < 1$, the cationic ligands repel each other and the binding is anti or negatively cooperative; when $\omega = 1$, neither cooperativity is observed during the binding.

Schwarz's theory also implies two types of intrinsic binding processes: (1) the binding of isolated ligands with binding

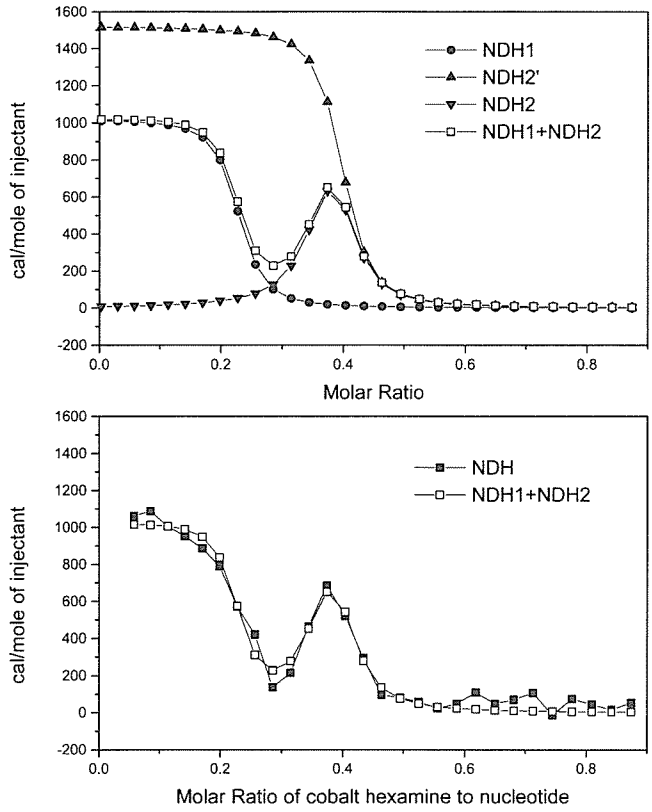

Figure 6. Optimum fitting for the experimental ITC curve (■) of $Co(NH_3)_6^{3+}$/pDNA, NDH1 + NDH2 (□). NDH1 (●) represents the initial binding stage corresponding to that in Figure 4. NDH2′ (▲) and NDH2 (▼) are the same as those in Figure 5. NDH1 + NDH2 is used for the fitting of the experimental ITC curve; $N_1 = 0.216 \pm 0.004$, $K_1 = (17.79 \pm 4.99) \times 10^5\ M^{-1}$, $\Delta H_1 = 1019 \pm 30$ cal/mol, $N_2' = 0.385 \pm 0.012$, $N_3 = 0.354$, $N_2 = N_2' - N_3 = 0.031 \pm 0.012$, $K_2 = K_2' = (27.82 \pm 12.61) \times 10^5\ M^{-1}$, $\Delta H_2 = \Delta H_2' = 1520 \pm 301$ cal/mol.

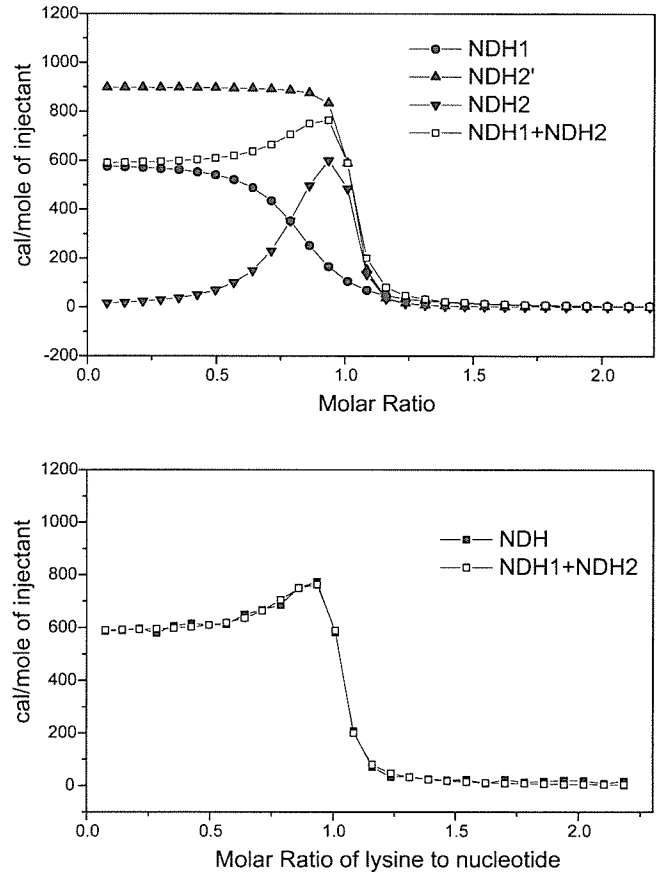

Figure 7. Optimum fitting for the experimental ITC curve (■) of PEG−PLL/pDNA, NDH1 + NDH2 (□). NDH1 (●) represents the initial binding stage corresponding to those of the PEG−PLL/pDNA system shown in Figures 5 and 6. NDH2′ (▲) and NDH2 (▼) correspond to those in Figure 6. NDH1 + NDH2 is used for the fitting of the experimental ITC curve: $N_3 = N_1 = 0.810 \pm 0.026$, $K_1 = (2.66 \pm 0.62) \times 10^5\ M^{-1}$, $\Delta H_1 = 585 \pm 5$ cal/mol, $N_2' = 0.994 \pm 0.005$, $N_2 = N_2' - N_3 = 0.184 \pm 0.031$, $K_2 = K_2' = (51.07 \pm 13.98) \times 10^5\ M^{-1}$, $\Delta H_2 = \Delta H_2' = 899 \pm 37$ cal/mol.

constant K (nucleation), and (2) the binding of ligands to the nearest-neighbor binding site (aggregation) with binding constant Kq, where q is the cooperativity parameter. In both models, the binding process with the binding constant $K\omega$ or Kq is generated by the initial ligand binding with binding constant K, which is the matter of our concern. Let us assume that K_2 was equal to $K\omega$ or Kq. For the cobalt hexamine binding to DNA, ω or q is estimated to be 1.56, which is obtained by K_2/K_1 using the parameters shown in Table 1. For the PEG−PLL binding to DNA, ω or q is estimated to be 19.20 using the parameters shown in Table 2. In both cases, it is obvious that the binding constant K_2 seems to be significantly enhanced and the estimation for the cobalt hexamine binding is inconsistent with the reported data.[2] Although the above classification was suggested to explain the cooperative binding of the cationic ligands, it is not clear in this study whether such kinds of cooperativities induced by the ligand−ligand interactions exist in the binding of the cobalt hexamine or PEG−PLL to pDNA.

In this study, it was assumed that the positive cooperative binding of the cobalt hexamine or PEG−PLL to DNA is attributed to the conformational change in DNA rather than the interaction between the same chemicals. The DNA conformational change produces the environmental modulation around the DNA vicinity, and this may affect the binding features of the cationic ligands. Hud et al. suggested that the effect of the DNA segment fluctuation induces the enhanced binding of cationic ligands to a loop formed by two sequence-separated sections in close contact.[25] The cationic ligands bind to this contact and stabilize the loop. Successive ligands bind both the loop and extended DNA to induce the collapsed form. Therefore, the binding constants K_1 and K_2 are treated as individual variables in this study.

To develop a flexible fitting method, different types of ligands, a low-molecular weight metal complex cobalt hexamine and block copolymer PEG−PLL, were employed in this study. Cobalt hexamine is a widely used chemical as a standard reagent of DNA condensation. On the contrary, PEG−PLL is a relatively recently developed reagent as a gene carrier.[19] As exemplified by the presence or absence of the delay in the appearance of the second binding stage in Figures 2 and 3, the condensation mechanism seems to be slightly different from each other despite the same driving force, the electrostatic interaction. It was reported that this difference becomes enhanced in the dilute DNA solution experiments and the latter more effectively induces the DNA condensation.[21]

Under such situations, the charge equivalent mixing ratio between PEG−PLL and DNA is enough to induce the DNA condensation, while an excess amount of cobalt hexamine, at least several times that of the phosphate residue, should be required. A similar trend was observed in the ITC curves obtained in this study. The charge ratio at the end point of the PEG−PLL titration was 1.2, while that of cobalt hexamine was slightly higher than this value. This difference was mainly caused by their chemical structures. In this study, a simple comparison of the thermodynamic parameters N_1 and K_1 in the

TABLE 1: Parameters Obtained by Various Fitting Methods

	N_1	$K_1/10^5$ (M^{-1})	ΔH_1 (cal/mol)	N_2	$K_2/10^5$ (M^{-1})	ΔH_2 (cal/mol)
this work[a]	0.216 ± 0.004	17.79 ± 4.99	1019 ± 30	0.031 ± 0.012	27.82 ± 12.61	1520 ± 301
ref 2[b]	0.217 ± 0.012	2.30 ± 0.80	1240 ± 100	0.059 ± 0.012	6.00 ± 1.60	820 ± 90
origin[c]	0.218 ± 0.010	74.02 ± 142.4	1086 ± 68	not converged		

[a] This work: developed by this work. [b] ref 2: reported in reference 2. [c] Origin: by applying the two sets of independent sites (TSIS) model to each binding process divided from the experimental ITC curve shown in Figure 2, which is the same method as that used in the ref 2. $N_2' = 0.385 \pm 0.012$, $N_3 = 0.354$, N_2 ($=N_2' - N_3$) $= 0.031 \pm 0.012$, $K_2 = K_2'$, $\Delta H_2 = \Delta H_2'$.

TABLE 2: Parameters Obtained by Various Fitting Methods

	N_1	$K_1/10^5$ (M^{-1})	ΔH_1 (cal/mol)	N_2	$K_2/10^5$ (M^{-1})	ΔH_2 (cal/mol)
this work[a]	0.810 ± 0.026	2.66 ± 0.62	585 ± 5	0.184 ± 0.031	51.07 ± 13.98	899 ± 37
origin[b]	0.781 ± 0.032	139.10 ± 44.19	584 ± 9	0.222 ± 0.034	7.2 ± 2.23	973 ± 77

[a] This work: developed by this work. [b] Origin: by applying TSIS model to the ITC curve shown in Figure 3. $N_3 = N_1$, $N_2' = 0.994 \pm 0.005$, N_2 ($=N_2' - N_3$) $= 0.184 \pm 0.031$, $K_2 = K_2'$, $\Delta H_2 = \Delta H_2'$.

cobalt hexamine system with those of PEG−PLL makes no realistic sense, because the former was analyzed in a molar unit and the latter was summarized in a charge unit. On comparison of N_1 with the consideration of the valency, however, it is obvious that PEG−PLL more effectively binds (see Tables 1 and 2).

In the novel fitting model developed in this study, the cationic ligand binding to DNA was classified into two stages, the initial and second binding stages. The former has the binding constant K_1 and the latter K_2. Regarding the magnitude relationship of the binding constants, Teif and Lando theoretically pointed out that the DNA conformational change to the collapsed state takes place when $K_2 > K_1$.[16] In the general curve fitting models for the experimental ITC curves, however, this assumption could not be taken into consideration. Although general fitting models that can treat multiple binding sites have the assumption $K_1 > K_2$, our model is not restricted by this assumption. To treat two binding stages as individual events, they were characterized in relation to the conformational change in pDNA. Thus, the former occurs when the DNA conformation retained as the elongated state and the latter is promoted during the DNA conformational change.

Generally, there is a significant difficulty in the separation of the two binding stages, when the overlap of the initial and second binding stages was observed as shown in the PEG−PLL system. Despite the absence of the saddle point in the integrated ITC curve for the PEG−PLL system, the assumption of two-stage binding is plausible, because the discrete transition between the elongated and collapsed states was essentially the same as that observed in the cobalt hexamine system.[21] Table 1 shows a comparison of the thermodynamic parameters determined in this study with those by other methods reported in ref 2 and obtained by the manufacturer recommended method that is based on the two sets of independent sites (TSIS) model. Although the second set of parameters did not converge using the TSIS model, no significant difference was observed in both values of N_1 and N_2. As mentioned in the Introduction, the TSIS model should not be applied to the particular system where K_1 is smaller than K_2, because this model is constructed assuming that K_1 is greater than K_2. This is the reason the second set of parameters was not determined by the TSIS model.

Matulis et al. also employed the TSIS model, but they completely divided the integrated ITC curve by the saddle point. In their method, two parts of the ITC curve were separately fitted.[2] Therefore, the magnitude relationship of K_1 and K_2 would not be discussed under their framework. On the contrary, both parts were simultaneously fitted in this study. In addition, when their method was applied to the PEG−PLL system, the curve fitting was done under the restricted assumption $K_1 > K_2$. However, our method is not restricted by this assumption. Among these three methods, thus, an appropriate method suitable for the discussion on the magnitude relationship of K_1 and K_2 is considered to be limited to the novel method developed in this study.

The charge ratio of the cationic ligands to DNA is expressed by the total stoichiometry, the sum of N_1 and N_2. On the basis of the consideration of the valence of cobalt hexamine, the charge ratio is estimated to be 0.72 in this study, suggesting that the residual ligands do not directly contribute to the DNA condensation (see Table 1). This trend is consistent with another report.[2] It is still controversial that the results of the ITC experiments disagree with the theoretical prediction of the two-variable counterion condensation theory.[14] As for the PEG−PLL system, the charge ratio was determined to be 0.99, indicating that almost all of the negative charge of the DNA phosphate is neutralized by the ligand binding (see Table 2). The result of the charge equivalent complexation agrees with those obtained from the single molecule observation under fluorescence microscopy.[20] This difference in the binding stoichiometry between cobalt hexamine and PEG−PLL reflects the strength of the electrostatic interaction between the cationic ligands and DNA phosphates.

Conclusion

The novel fitting method based on the SSIS model for the experimental ITC curve was developed and applied to the cationic ligands binding to DNA, cobalt hexamine, and PEG−PLL systems in this study. It is demonstrated that this curve fitting method can be applicable for both systems. As for the cobalt hexamine system, the thermodynamic parameters obtained by the novel fitting method have a similar trend with those reported by other researchers. It was suggested that this method is applicable for the PEG−PLL system, in which the separation of the two binding events is not enough for the appearance of the experimental ITC curve. Although other fitting methods are applicable under the restricted assumption $K_1 > K_2$, our method, unrestricted by this assumption, is widely applicable for both cases, $K_1 > K_2$ and $K_2 > K_1$.

Acknowledgment. We thank Mr. S. Fukushima of Nippon Kayaku Co., Ltd., Japan, for the kind donation of the PEG−PLL block copolymer. This work was partially supported by a grant-in-aid for scientific research from the Ministry of Education, Culture, Sports, Science, and Technology of Japan (MEXT), the Core Research Program for Evolutional Science and Technology (CREST) from the Japan Science and Technol-

ogy Agency (JST), and 21st century COE program "Human-Friendly Materials based on Chemistry" from MEXT.

References and Notes

(1) Spink, C. H.; Chaires, J. B. *J. Am. Chem. Soc.* **1997**, *119*, 10920−10928.

(2) Matulis, D.; Rouzina, I.; Bloomfield, V. A. *J. Mol. Biol.* **2000**, *296*, 1053−1063.

(3) Bronich, T.; Kabanov, A. V.; Marky, L. A. *J. Phys. Chem. B* **2001**, *105*, 6042−6050.

(4) Matulis, D.; Rouzina, I.; Bloomfield, V. A. *J. Am. Chem. Soc.* **2002**, *124*, 7331−7342.

(5) Pozharski, E.; MacDonald, R. C. *Biophys. J.* **2002**, *83*, 556−565.

(6) Keller, M.; Tagawa, T.; Preuss, M.; Miller, A. D. *Biochemistry* **2002**, *41*, 652−659.

(7) Keller M.; Jorgensen, M. R.; Perouzel, E.; Miller, A. D. *Biochemistry* **2003**, *42*, 6067−6077.

(8) Ehtezazi, T.; Rungsardthong, U.; Stolnik, S. *Langmuir* **2003**, *19*, 9387−9394.

(9) Rungsardthong, U.; Ehtezazi, T.; Bailey, L.; Armes, S. P.; Garnett, M. C.; Stolnik, S. *Biomacromolecules* **2003**, *4*, 683−690.

(10) Nisha, C. K.; Manorama, S. V. *Langmuir* **2004**, *20*, 2386-2396.

(11) Freire, E.; Mayorga, O. L.; Straume, M. *Anal. Chem.* **1990**, *62*, 950A-959A.

(12) ITC Data Analysis in Origin, Ver.5.0; MicroCal, Inc.: Studio City, CA, 1998; pp 73−78.

(13) (a) Oosawa, F. *Polyelectrolytes*; Marcel Dekker: New York, 1971. (b) Manning, G. S. *Q. Rev. Biophys.* **1978**, *11*, 179−246.

(14) Wilson, R. W.; Bloomfield, V. A. *Biochemistry* **1979**, *18*, 2192−2196.

(15) Yamasaki, Y.; Teramoto, Y.; Yoshikawa, K. *Biophys. J.* **2001**, *80*, 2823−2832.

(16) Teif, V. B.; Lando, D. Y. *Mol. Biol.* **2001**, *35*, 106−107.

(17) Mel'nikov, S. M.; Sergeyev, V. G.; Yoshikawa, K. *J. Am. Chem. Soc.* **1995**, *117*, 9951−9956.

(18) Bloomfield,V. A. *Curr. Opin. Struct. Biol.* **1996**, *6*, 334−341.

(19) Katayose, S.; Kataoka, K. *Bioconjugate Chem.* **1997**, *8*, 702−707.

(20) Harada A.; Kataoka K. *Macromolecules* **1995**, *28*, 5294−5299.

(21) Yamasaki, Y.; Katayose, S.; Kataoka, K.; Yoshikawa, K. *Macromolecules* **2003**, *36*, 6276−6279.

(22) Yoshikawa, K.; Kidoaki, S.; Takahashi, M.; Vasilevskaya, V. V.; Khokhlov, A. R. *Ber. Bunsen-Ges. Phys. Chem.* **1996**, *100*, 876−880.

(23) McGhee, J. D.; von Hippel, P. H. *J. Mol. Biol.* **1974**, *86*, 469−489.

(24) Schwarz, G. *Eur. J. Biochem.* **1970**, *12*, 442−453.

(25) Hud, N. V.; Downing, K. H.; Balhorn, R. *Proc. Natl. Acad. Sci. U.S.A.* **1995**, *92*, 3581−3585.

J|A|C|S
COMMUNICATIONS

Published on Web 04/12/2006

Semipermeable Polymer Vesicle (PICsome) Self-Assembled in Aqueous Medium from a Pair of Oppositely Charged Block Copolymers: Physiologically Stable Micro-/Nanocontainers of Water-Soluble Macromolecules

Aya Koide,[†] Akihiro Kishimura,[†,‡,§] Kensuke Osada,[†,§] Woo-Dong Jang,[†,‡,||] Yuichi Yamasaki,[†,‡,§] and Kazunori Kataoka*[,†,‡,§]

Department of Materials Engineering, Graduate School of Engineering, and Center for NanoBio Integration, The University of Tokyo, 7-3-1 Hongo, Bunkyo-ku, Tokyo 113-8656 Japan, and CREST, Japan Science and Technology Agency, Japan

Received November 24, 2005; E-mail: kataoka@bmw.t.u-tokyo.ac.jp

Polymer vesicles enclosing a volume with a molecularly thin membrane, known as "polymersomes", have recently been attracting progressive attention from both fundamental and applied standpoints as carriers or containers for various functionality compounds.[1,2] Particularly, in an aqueous entity, amphiphilic block copolymers have been used for the preparation of polymersomes,[1-3] revealing unique characteristics such as high structural stability compared to conventional liposomes made from low molecular amphiphiles.[1] Very recently, stable encapsulation of biologically relevant substances, including drugs and enzymes, into the polymersomes has been directed to applications as delivery and bioreactor systems.[2] Nevertheless, the hydrophobic nature of the membrane in such amphiphilic polymersomes prevents the penetration of hydrophilic solutes, limiting their functionality as semipermeable container systems. Furthermore, the harsh preparation conditions, including the use of organic solvents, may hamper the encapsulation of fragile compounds such as proteins. Herein, we report for the first time the preparation of stable polymersomes with a semipermeable membrane through a simple mixing of a pair of oppositely charged block copolymers in an aqueous medium. The polymersome formed in this way is a new entity of polymer vesicles with a polyion complex (PIC) membrane and thus may be given a new terminology as a "PICsome".

A PICsome as a hollow sphere needs the formation of a stable layer of PIC lamellae as the partition membrane. In this regard, oppositely charged segments of the block copolymer pair are preferred to have a matched chain length, compensating for the counter charge in a stoichiometric manner and minimizing the phase mixing of the PIC middle layer with the outer and inner shell layers of the hydrophilic segment, in this case, poly(ethylene glycol) (PEG). Here, to satisfy this condition of matched chain length, both anionic and cationic block copolymers were prepared from the same platform polymer, PEG-poly(β-benzyl-L-aspartate) (PEG-PBLA), to have identical molecular weight and composition (Scheme 1). Two types of PEG-PBLA with a different PBLA composition (degree of polymerization (DP) of PBLA; 17 and 100) were prepared by the ring opening polymerization of β-benzyl-L-aspartate *N*-carboxyanhydride initiated from the ω-primary amino group of $CH_3O-PEG-NH_2$ (M_n = 2000, M_w/M_n = 1.05).[4] The anionic component of the PICsome, PEG-poly(α,β-aspartic acid) (PEG-P(Asp)$_{17}$ and PEG-P(Asp)$_{100}$), was obtained from PEG-PBLA by alkali hydrolysis as reported previously.[5] Alternatively, the cationic

Scheme 1. Synthesis of a Pair of Oppositely Charged Block Copolymers

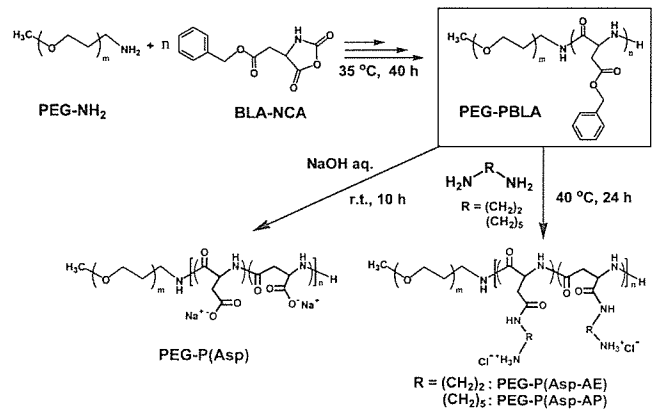

component was prepared from PEG-PBLA by aminolysis of flanking benzyl ester groups with an excess amount of diamine. A notable property of PBLA is that the benzyl ester groups can easily undergo quantitative aminolysis reactions with various diamines at ambient temperature via the formation of a succinimidyl ring structure as an intermediate, allowing the preparation of cationic poly(aspartamide)s with different amine functionalities. Indeed, quantitative aminolysis was confirmed from ^{1}H NMR spectra.[4] Two types of diamines with a different number of methylene units, 1,2-diaminoethane and 1,5-diaminopentane, were used in the aminolysis to obtain PEG-poly([2-aminoethyl]-α,β-aspartamide) (PEG-P(Asp-AE)$_{17}$ and PEG-P(Asp-AE)$_{100}$) and PEG-poly([5-aminopentyl]-α,β-aspartamide) (PEG-P(Asp-AP)$_{17}$ and PEG-P(Asp-AP)$_{100}$), respectively, to explore the effect of the alkyl-spacer length on the self-assembly behavior.

The anionic and cationic block copolymers were separately dissolved in 10 mM Tris-HCl buffer (pH 7.4) with a physiological salt concentration of 150 mM NaCl. Both solutions were then mixed in an equal ratio of $-COO-$ and $-NH_3^+$ units to form PIC and subsequently subjected to sonication.[4] Flow particle image analysis[4] and dark-field microscopic (DFM) observation suggested the formation of spherical particles with the diameter up to 10 μm in the PEG-P(Asp)$_{100}$/PEG-P(Asp-AP)$_{100}$ system (Figure 1), which is obviously with a larger size range than that of the well-documented PIC micelles with a core−shell architecture.[6] The DFM image was more fascinating, showing characteristic ringlike scatterings (Figure 1), suggesting the hollow structure of the particles. Note that the scattering light intensity in DFM correlates with the density of the objects, giving a ringlike image for hollow particles with a large density difference between the inner and peripheral regions.[7] The

[†] Department of Materials Engineering, Graduate School of Engineering, The University of Tokyo.
[‡] CREST, Japan Science and Technology Agency.
[§] Center for NanoBio Integration, The University of Tokyo.
[||] Present address: Department of Chemistry, Yonsei University, Korea.

10.1021/ja057993r CCC: $33.50

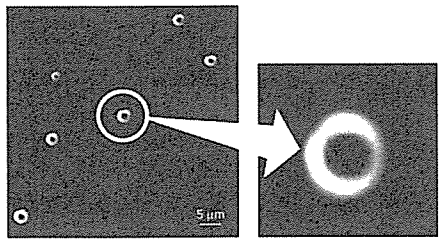

Figure 1. Dark-field microscopic images of PICsomes prepared from a PEG-P(Asp)$_{100}$/PEG-P(Asp-AP)$_{100}$ system.

balance of the segment length in the block copolymer is expected to play a substantial role in the self-assembly process. Indeed, the combination of the block copolymers with a shorter charged segment, PEG-P(Asp)$_{17}$/PEG-P(Asp-AP)$_{17}$ system, gave a DFM image with only few ring-scattering objects dispersed in the major part of the small dot scatterings presumably from micelles. Block copolymers with shorter charged segments compared to the PEG segment adopt a cone-shaped conformation preferring the micelle architecture.[6] The molecular shape gradually changes from cone to rod with the increased length of the charged segments relative to the PEG segments, and eventually, the assembly should adopt the vesicular structure with a smaller curvature than the spherical micelle.[8] The observations here are consistent with this general rule of vesicular formation through molecular assembly. Another factor influencing the vesicular formation seems to be the alkyl-spacer length of the cationic side chain of the poly(aspartamide) segment, which may be related to the flexibility of the ion pair formed in the PIC structure. A decrease in the alkyl-spacer length from pentyl to ethyl in the side chain of the cationic poly(aspartamide) segment, viz. the PEG-P(Asp)$_{100}$/PEG-P(Asp-AE)$_{100}$ system, resulted in a significant decrease in the size (<1 μm) of the ring scatterings observed in DFM. It is likely that the length of the alkyl spacer may be a critical factor in determining the stable PICsome size, yet a further detailed study should be needed to confirm this assumption.

The hollow structure of the large PIC assembly from PEG-P(Asp)$_{100}$/PEG-P(Asp-AP)$_{100}$ system as "PICsome" was further directly evidenced from the encapsulation of the water-soluble macromolecule labeled with fluorescein isothiocyanate, FITC-dextran (FITC-Dex, M_n = 40 000), into the PICsome. Cross-sectional observation by the confocal laser scanning microscope (CLSM) clearly confirmed the successful inclusion of FITC-Dex into the PICsome by a simple mixing of PEG-P(Asp-AP)$_{100}$ (1 mg/mL) with PEG-P(Asp)$_{100}$ (1 mg/mL) containing FITC-Dex (1 mg/mL) (Figure 2).[4] The PICsome with encapsulating FITC-Dex was appreciably stable in physiological buffer as observed by CLSM even after 3 months standing at ambient temperature.

The semipermeability of the PICsome membrane was then investigated using fluorescent molecules with different molecular weights. The fluorescence collected through the objective lens was resolved by the diffraction grating and monitored by a 32-channel arrayed detector. Upon addition of dextran labeled with tetramethylrhodamine isothiocyanate (TRITC-Dex, M_n = 70 000) to the solution of PICsome with encapsulated FITC-Dex, a green fluorescence of FITC inside the PICsome was clearly observed, sharply discriminated from the red fluorescence of TRITC-Dex in the outer medium, in the merged image of CLSM taken at the excitation wavelength for FITC and TRITC (488 and 543 nm) (Figure 2a). On the other hand, upon addition of free TRITC (MW = 443.5) to the solution of the FITC-Dex encapsulating PICsome, a yellow color was observed inside the PICsome (Figure 2b).[4] An emission spectrum of the region of interest (ROI) in Figure 2b shows the

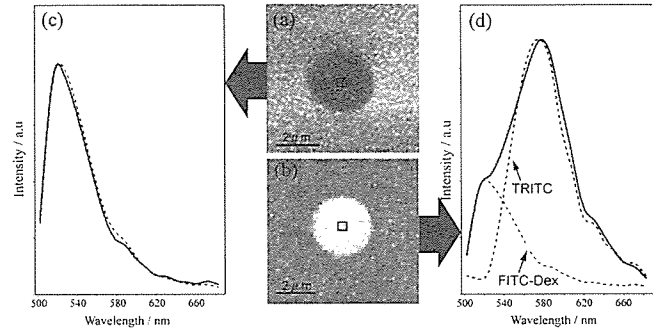

Figure 2. CLSM images and emission spectra of PICsome encapsulating FITC-Dex. Images after the addition of (a) TRITC-Dex or (b) TRITC. (c) Spectra of the ROI in (a) after (solid line) and before (blue dotted line) the addition of TRITC-Dex. (d) A spectrum of the ROI in (b) (solid line) with reference spectra of FITC-Dex (green dotted line) and TRITC (red dotted line).

intense fluorescence with the maximum at 580 nm and the shoulder at 520 nm (Figure 2d). The profile was reasonably fitted with both references of FITC-Dex and TRITC, indicating the penetration of TRITC into the PICsome interior. In contrast, the spectrum of the ROI in Figure 2a corresponds to the spectrum of FITC-Dex before the addition of TRITC-Dex (Figure 2c), indicating the segregation of TRITC-Dex from the PICsome interior. These results visually demonstrated the semipermeable character of the PIC membrane. Notably, the PICsome was able to retain its vesicular structure in the presence of a colloidal osmotic pressure of approximately 10 μOsm from the encapsulated FITC-Dex and was stable even in the medium containing 10% fetal bovine serum at 37 °C,[4] being feasible for biomedical applications.

In summary, a novel entity of a polymer vesicle, a PICsome, was prepared here by a simple mixing of a pair of oppositely charged block copolymers composed of biocompatible PEG and poly(amino acid)s in an aqueous medium. The PICsome is stable in proteinous medium and has a partition membrane with a unique three-layered structure. These biocompatible composition and biologically relevant characteristics of the PICsomes may open their future utility in biomedical fields such as carriers of therapeutic compounds and compartments for diagnostic enzymes.

Acknowledgment. We thank Prof. K. Akiyoshi and Dr. S. M. Nomura (Tokyo Medical and Dental University) for valuable suggestions for DFM observation and Mr. F. Ishidate (Carl Zeiss Co., Ltd.) for emission spectrum measurements.

Supporting Information Available: Syntheses, characterizations, and preparations of PICsomes. This material is available free of charge via the Internet at http://pubs.acs.org.

References

(1) (a) Discher, D. E.; Eisenberg, A. *Science* **2002**, *297*, 967−973. (b) Geng, Y.; Ahmed, F.; Bhasin, N.; Discher, D. E. *J. Phys. Chem. B* **2005**, *109*, 3772−3779. (c) Antonietti, M.; Förster, S. *Adv. Mater.* **2003**, *15*, 1323−1333.
(2) Brož, P.; Benito, S. M.; Saw, C.-L.; Burger, P.; Heider, H.; Pfisterer, M.; Marsch, S.; Meier, W.; Hunziker, P. *J. Control. Release* **2005**, *102*, 475−488. (b) Ranquin, A.; Versées, W.; Meier, W.; Steyaert, J.; Van Gelder, P. *Nano Lett.* **2005**, *5*, 2220−2224.
(3) (a) Bellomo, E. G.; Wyrsta, M. D.; Pakstis, L.; Pochan, D. J.; Deming, T. J. *Nat. Mater.* **2004**, *3*, 244−248. (b) Rodoríguez-Hernández, J.; Lecommandoux, S. *J. Am. Chem. Soc.* **2005**, *127*, 2026−2027.
(4) See Supporting Information.
(5) Yokoyama, M.; Inoue, S.; Kataoka, K.; Yui N.; Okano, T.; Sakurai, Y. *Makromol. Chem.* **1989**, *190*, 2041−2054.
(6) (a) Harada, A.; Kataoka, K. *Macromolecules* **1995**, *28*, 5294−5299. (b) Harada, A.; Kataoka, K. *Science* **1999**, *283*, 65−67. (c) Kataoka, K.; Harada, A.; Nagasaki, Y. *Adv. Drug Delivery Rev.* **2001**, *47*, 113−131.
(7) Hotani, H. *J. Mol. Biol.* **1984**, *178*, 113−120.
(8) Zhang, L.; Eisenberg, A. *J. Am. Chem. Soc.* **1996**, *118*, 3168−3181.

JA057993R

Biological Chemistry

DOI: 10.1002/anie.200504441

Intracellular Inducible Alkylation System That Exhibits Antisense Effects with Greater Potency and Selectivity than the Natural Oligonucleotide**

*Md. Monsur Ali, Motoi Oishi, Fumi Nagatsugi, Kenya Mori, Yukio Nagasaki, Kazunori Kataoka, and Shigeki Sasaki**

Synthetic oligonucleotides (ODNs) that incorporate a chemically reactive appendage have been widely investigated in the endeavor to create new functions through specific reactivity toward a target sequence. A number of biotechnological approaches have been invented based on sequence-selective alkylation,[1] cross-linking,[2,3] strand cleavage,[4–7] chemical ligation,[8] signal amplification,[9] and other techniques. Cross-linking oligonucleotides have been used to stabilize complexes with the cellular target mRNA by covalent-bond formation, and have been shown to be useful in enhancing antisense effects. Emerging knowledge about the fundamental role of micro-RNAs (miRNAs) in gene regulation has led to great interest in efficient antisense oligonucleotides against miRNAs as a tool for specifically knocking down particular miRNAs.[10,11] Psoralen derivatives are activated by UV irradiation and are the only reagents applicable to in vitro and in vivo studies. They not only enhance antisense effects[12,13] but also induce specific mutations at the sites of the reaction within the triplex DNA.[14,15] However, until now the use of alkylating oligonucleotides in biological studies has been hampered by the lack of an efficient cross-linking agent. As alkylating or cross-linking agents tend to be unstable under physiological conditions, the use of stable precursors with inducible reactivity was expected to provide a solution to this problem.[2,16] We recently proposed a new concept of inducible reactivity, in which a phenylsulfide derivative used as a stable precursor to a 2-amino-6-vinylpurine nucleoside analogue is automatically activated in the proximity of the target cytidine residue to form a covalent bond selectively (Scheme 1).[17–20] The selectivity of this inducible alkylation system for cytidine is so high that a single nucleotide difference can be discriminated in the alkylation. Herein we describe the capacity of the inducible alkylation system to exhibit antisense effects in an intracellular environment with greater potency and selectivity than the corresponding unmodified oligonucleotide.

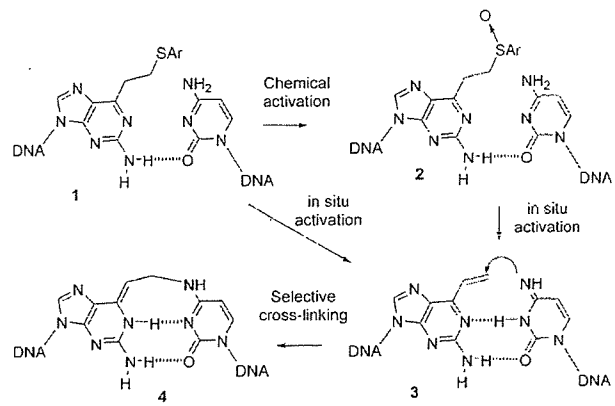

Scheme 1. In situ activation of the sulfide precursor **1** to the 2-amino-6-vinylpurine **3** for selective cross-linking with cytidine to give **4**.[17] The vinyl compound **3** can be generated selectively in the hybrid with the complementary sequence from the sulfoxide **2** or the sulfide precursor **1**. As intermediary formation of **2** has not been detected, it is anticipated that activation from **1** to **3** takes place directly.

In a previous study, the phenylsulfide derivative **1** was oxidized chemically to produce the sulfoxide derivative **2**, which was activated selectively to the vinyl compound **3** by hybridization with the complementary sequence. It has been shown that the cytidine residue at the target site enhances the elimination step from **2** to **3**, which is followed by efficient

[*] Dr. M. M. Ali, Prof. Dr. F. Nagatsugi, Prof. Dr. S. Sasaki
Graduate School of Pharmaceutical Sciences
Kyushu University
3-1-1 Maidashi, Higashi-ku, Fukuoka 812-8582 (Japan)
Fax: (+81) 92-642-6615
E-mail: sasaki@phar.kyushu-u.ac.jp
Dr. M. Oishi, Prof. Dr. Y. Nagasaki
Institute of Materials Science
Tsukuba University
1-1-1 Ten-nodai, Tsukuba, Ibaraki 305–8573 (Japan)
Dr. K. Mori
GeneAct Ltd.
2432-3 Kawaimachi, Kurume, Fukuoka 839-0861 (Japan)
Prof. Dr. K. Kataoka
Department of Materials Science and Engineering
Graduate School of Engineering
The University of Tokyo
7-3-1 Hongo, Bunkyo-ku, Tokyo 113-8656 (Japan)

[**] This work was supported by a Grant-in-Aid for Scientific Research (A) from the Japan Society for the Promotion of Science (JSPS) and CREST of the Japan Science and Technology Agency (JST).

Supporting information for this article is available on the WWW under http://www.angewandte.org or from the author.

alkylation to produce 4.[17] The vinyl compound **3** can also be generated selectively from the sulfide precursor **1** in the hybrid with the complementary sequence. In this case it is anticipated that activation from **1** to **3** takes place directly. The elimination of the sulfide group is also accelerated by the cytidine residue at the target site. As the sulfide derivative **1** is chemically stable, we viewed it as a potential candidate for an alkylating agent with inducible reactivity for use in living systems.

Herein, we have applied polyion-complex (PIC) micelles of PEG conjugates of oligonucleotides for both the protection of ODNs from enzymatic digestion and their efficient delivery into the cellular interior.[21–23] Scheme 2 summarizes the

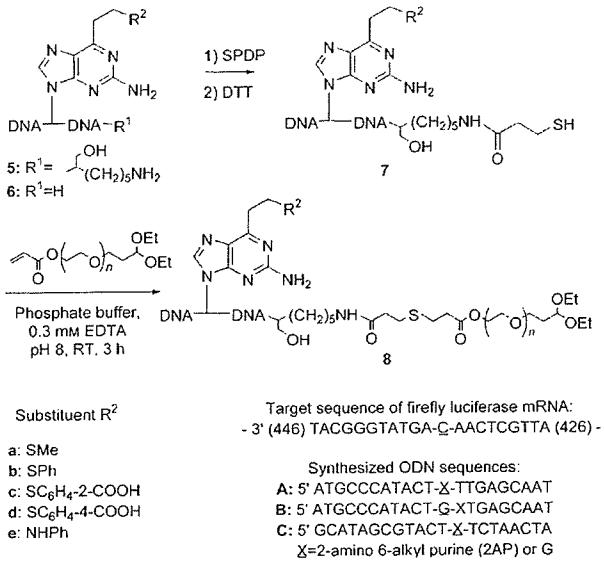

Scheme 2. Synthesis of the antisense PEG conjugates in which 2-amino 6-alkyl purine is incorporated. The sequence **A** has X at the complementary site to the cytidine residue of the target mRNA sequence, **B** contains X at the adjacent site, and **C** is a random sequence. The description **6A** refers to species with the ODN sequence **A** that are not conjugated with PEG; **8B** (X = AP, R^2 = SMe) is the PEG conjugate with the ODN sequence **B** in which a 2-amino-6-(2-methylthioethyl)purine derivative is incorporated adjacent to the complementary site to the cytidine residue of the target sequence. EDTA = ethylenediaminetetraacetic acid.

synthesis of PEG conjugates of the functional oligonucleotides. The antisense sequence to firefly-luciferase mRNA (sequence **A** in Scheme 2) was designed according to a reported technique.[24] The methylsulfide derivative of a 2-amino 6-alkyl purine was incorporated into the natural-type ODN (**5a** and **6a**),[17] and was then transformed into the phenylsulfide (**5b**, **6b**), 2-carboxyphenylsulfide (**5c**, **6c**), 4-carboxyphenylsulfide (**5d**, **6d**), and phenylamino derivatives (**5e**) by sequential reactions with magnesium monoperphthalate (MMPP) and aqueous NaOH, following the addition of the corresponding thiol or amine. The amino group of the 3′ terminus of **5** was modified with *N*-succimidyl-3-(2-pyridyldithio)propionate (SPDP), followed by reduction with dithiothreitol (DTT) to form the thiol-containing ODN **7**. Finally, the β-thiopropionate linkage of the corresponding ODN-PEG conjugates **8** was formed by a Michael reaction with a PEG polymer bearing a diethylacetal group at one terminus and an acrylate group at the other (M_n = 4460). The conjugates **8** were isolated in good yields by purification by reversed-phase column chromatography. Sequence **A** has X at the complementary site to the cytidine residue of the target mRNA sequence, **B** contains X at the adjacent site, and **C** is a random sequence. The structures of the ODNs and the PEG conjugates were confirmed by MALDI-TOF MS. The PEG–ODN conjugates obtained were mixed with poly-L-lysine (PLL) in a 1:1 molar ratio with respect to the phosphate group in the PEG–ODN conjugate and the amino group in PLL to form the PIC micelles (N/P = 1).

Antisense effects of the reactive ODNs (**6A**, R^1 = H) were first evaluated in a transcription and translation assay without cells. The following order was found for the cross-linking rates of the derivatives of 2-aminopurine in the nonbiological system: phenyl sulfoxide > 2-carboxyphenylsulfide ≫ phenylsulfide > methylsulfide.[17] However, as the phenyl sulfoxide derivatives were found to be unstable in the biological assay, the sulfide-functionalized ODNs were used in this study. Transcription, followed by translation, of firefly luciferase was performed by using ODN **6** (X = G or a sulfide derivative of 2-aminopurine) and firefly-luciferase DNA in a wheat-germ extract. Production of luciferase was monitored by measuring luminescence (Figure 1). All ODNs **6A** showed dose-dependent antisense inhibition. It should be noted that all sulfide-functionalized ODNs showed higher antisense effects than the corresponding natural antisense ODN.

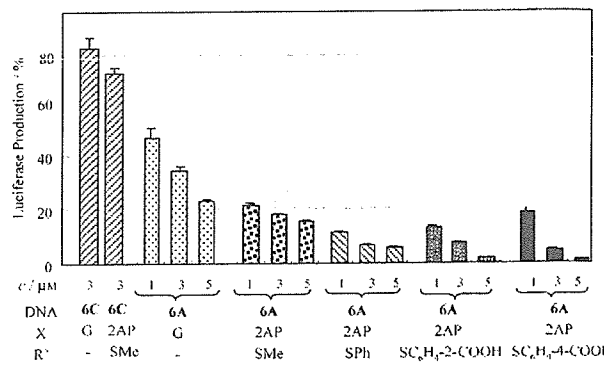

Figure 1. Antisense effects on luciferase production in an assay without cells. Transcription and translation were performed in vitro for 90 min at 30 °C by using DNA (0.3 μg) in the absence or presence of the ODN in TNT coupled wheat germ extract system (Promega). The extent of luciferase production relative to that in the control is shown in the ordinate.

To check whether or not in situ activation would take place in a cell lysate, we mixed the reactive ODN **6A** (X = AP, R^2 = SMe) and the ODN with the target sequence in a cell lysate, and the reaction mixture was analyzed by HPLC.[25] Although the cross-linked adduct was not detected clearly, the formation of 2-amino-6-vinylpurine was evidenced by its intrinsic fluorescence. This vinyl derivative of ODN **6** was

